Received: 6 September 2023 | Revised: 15 January 2024 | Accepted: 19 January 2024

DOI: 10.1002/glia.24512

GLIA

WILEY

RESEARCH ARTICLE

Aquaporin-4 and transient receptor potential vanilloid 4 balance in early postnatal neurodevelopment

Antonio Cibelli[1] | Maria Grazia Mola[1] | Emanuela Saracino[2] | Barbara Barile[1] | Pasqua Abbrescia[3] | Guido Mogni[1] | David C. Spray[4] | Eliana Scemes[5] | Andrea Rossi[6] | Diletta Spennato[2] | Maria Svelto[1] | Antonio Frigeri[3,4] | Valentina Benfenati[2] | Grazia Paola Nicchia[1,2,4]

[1]Department of Biosciences, Biotechnology and Environment, University of Bari Aldo Moro, Bari, Italy

[2]Institute for Organic Synthesis and Photoreactivity (ISOF), National Research Council of Italy (CNR), Bologna, Italy

[3]Department of Translational Biomedicine and Neuroscience, University of Bari Aldo Moro-Medical School, Bari, Italy

[4]Department of Neuroscience, Albert Einstein College of Medicine, Bronx, New York, USA

[5]Department of Cell Biology and Anatomy, NY Medical College, Valhalla, New York, USA

[6]Genome Engineering and Model Development Lab (GEMD), IUF-Leibniz Research Institute for Environmental Medicine, Düsseldorf, Germany

Correspondence
Grazia Paola Nicchia, Department of Biosciences, Biotechnology and Environment, University of Bari Aldo Moro, Via Orabona 4, 70125 Bari, Italy.
Email: graziapaola.nicchia@uniba.it

Funding information
Next Generation EU (National Recovery and Resilience Plan), Grant/Award Numbers: CN00000041, PE12, PE8; Universita degli Studi di Bari Aldo Moro, Grant/Award Number: HORIZON EUROPE SEEDS INTERGLIO (S08); European Commission, Grant/Award Number: ASTROTECH (GA956325); Air Force Office of Scientific Research (AFOSR), Grant/Award Numbers: FA9550-19-1-0370, FA9550-20-1-0324, FA9550-21-1-00352, FA9550-23-1-0583, FA9550-20-1-0386, FA9550-23-1-0736

Abstract

In the adult brain, the water channel aquaporin-4 (AQP4) is expressed in astrocyte endfoot, in supramolecular assemblies, called "Orthogonal Arrays of Particles" (OAPs) together with the transient receptor potential vanilloid 4 (TRPV4), finely regulating the cell volume. The present study aimed at investigating the contribution of AQP4 and TRPV4 to CNS early postnatal development using WT and AQP4 KO brain and retina and neuronal stem cells (NSCs), as an in vitro model of astrocyte differentiation. Western blot analysis showed that, differently from AQP4 and the glial cell markers, TRPV4 was downregulated during CNS development and NSC differentiation. Blue native/SDS-PAGE revealed that AQP4 progressively organized into OAPs throughout the entire differentiation process. Fluorescence quenching assay indicated that the speed of cell volume changes was time-related to NSC differentiation and functional to their migratory ability. Calcium imaging showed that the amplitude of TRPV4 Ca^{2+} transient is lower, and the dynamics are changed during differentiation and suppressed in AQP4 KO NSCs. Overall, these findings suggest that early postnatal neurodevelopment is subjected to temporally modulated water and Ca^{2+} dynamics likely to be those sustaining the biochemical and physiological mechanisms responsible for astrocyte differentiation during brain and retinal development.

Antonio Cibelli and Maria Grazia Mola should be considered joint first authors.

KEYWORDS
aquaporin-4, astrocytes, CNS development, glia differentiation, neuronal stem cells, orthogonal arrays of particles, transient receptor potential vanilloid 4

1 | INTRODUCTION

Central nervous system (CNS) development is an intricate process involving glial and neuronal differentiation and the formation of vascular plexuses, specific neuronal pathways, and functional synapses that underlie brain functions (Bautch & James, 2009; Rice & Barone, 2000; Saunders et al., 2012; Wise & Jones, 1976). Rodent brain development begins in the embryo at E11 and E9 in rats and mice, respectively, reaching ~90% of its adult weight at the end of the third week after birth (Rice & Barone, 2000; Semple et al., 2013). In the brain and retina, neurogenesis and gliogenesis originate from radial glia progenitors that guide the migration of young neurons and astrocytes toward their target layer (Beattie & Hippenmeyer, 2017; Bentivoglio & Mazzarello, 1999; Bringmann et al., 2006; Rakic, 2003; Raymond et al., 2006; Zecevic, 2004).

At birth, both the brain and retina are characterized by a large volume of extracellular space (ECS) that gradually decreases during postnatal development, due to cell proliferation (Nicholson & Hrabětová, 2017; Syková et al., 1998). The establishment of synapses and the intense neuronal activity alter ion and water homeostasis (Gardner-Medwin, 1983; Lehmenkühler et al., 1993). Astrocytes are actively involved in a large range of functions including the maintenance of homeostasis, metabolic support, regulation of blood flow, as well as neurotransmitter uptake and recycling during synaptic transmission (reviewed in Sofroniew & Vinters, 2010). Time course studies in postnatal rat cerebellum have indicated that the astrocytic water channel aquaporin-4 (AQP4) might play a crucial role in water and K^+ homeostasis from the second week of development when its expression markedly increases, specifically around blood vessels (Wen et al., 1999). Furthermore, AQP4 emerged as a crucial player in the multistep process of adult neurogenesis such as in cell migration, axonal sprouting, and synaptogenesis (Zheng et al., 2010), since its deletion greatly impairs cell proliferation and neuronal differentiation in adult stem cells (Kong et al., 2008; Küppers et al., 2008). AQP4 is a constitutively open water channel allowing bidirectional transport of water in response to osmotic gradients (Verkman et al., 2014) and it is expressed as well-ordered protein assemblies called "Orthogonal Arrays of Particles (OAPs)", visible by freeze-fracture electron microscopy (FFEM) (Furman et al., 2003), and more recently by super-resolution microscopy (Ciappelloni et al., 2019; Crane et al., 2008; Verkman et al., 2012). OAPs are formed by two isoforms called M1- and M23-AQP4 with similar water permeability but a different role in the OAP formation with M23-AQP4 selectively being the OAP forming isoform (de Bellis et al., 2021; Neely et al., 1999; Rash et al., 2004; Silberstein et al., 2004). Single-molecule tracking studies indicated that the M1-AQP4 isoform exhibits significantly greater mobility compared to M23-AQP4, which is confined to the core with low diffusion, influencing the overall structure and packing of OAPs. At OAP edges, a dynamic equilibrium exists between M1-AQP4 and M23-AQP4 tetramers, preventing excessive growth, and maintaining array organization (Ciappelloni et al., 2019; Crane et al., 2008; Verkman et al., 2012).

Different-sized OAPs play different roles in dynamic cellular events such as cell adhesion and migration (Hiroaki et al., 2006; Smith et al., 2014). Being motile in the cell plasma membrane, the M1-AQP4-based tetrameric form diffuses in lamellipodial regions, improving cell migration in physiological and pathological conditions (Smith et al., 2014). On the other hand, M23-AQP4 enriched OAPs promote cell adhesion and AQP4 polarization at the glial endfoot (Smith et al., 2014) and can influence the fate of glioma cells (Simone et al., 2019). Our recent studies on a CRISPR/Cas9 mouse model lacking the M23-AQP4 isoform and therefore unable to form OAPs (OAP-null mice) demonstrated that the absence of the M23 isoform not only leads to a complete depletion of OAPs but also a significant reduction in the total AQP4, highlighting the crucial role of OAP formation to ensure the physiological AQP4 expression level at glial endfeet (de Bellis et al., 2021).

AQP4 plays a central role in regulatory volume mechanisms by swiftly promoting water influx and efflux (Mola et al., 2016) occurring during cell swelling, shrinking as well as regulatory volume decrease (RVD) and increase (RVI). A range of studies have indicated that AQP-mediated cell swelling is required for the activation of the cation-permeable ion channel transient receptor potential vanilloid member-4 (TRPV4) (Benfenati et al., 2011; Jo et al., 2015; Liu et al., 2006; Mola et al., 2016; Toft-Bertelsen et al., 2017) co-expressed with AQP4 at glial endfeet. However, volume regulation is not exclusive of AQP4 and TRPV4 functional complex being TRPV4 a volume-sensor (Ritzmann et al., 2023; Toft-Bertelsen et al., 2017, 2018) reacting to cell volume increases irrespective of the specific molecular mechanisms triggering cell swelling, which can be prompted by osmotic changes via AQPs or other factors leading to an influx of water into the cell (Toft-Bertelsen et al., 2017). The coupling between TRPV4-mediated calcium influx and RVD is still unclear but likely coupled to downstream unidentified effectors, promoting the loss of electrolytes and water (Mola et al., 2016; Toft-Bertelsen et al., 2018). Furthermore, it has been shown that TRPV4 can affect AQP4 expression and modulate its gene transcription in vitro and in vivo (Jo et al., 2015; Lafrenaye & Simard, 2019; Salman et al., 2017).

The hypothesis of the present study is that the coordination between AQP4 expression level and aggregation state and TRPV4 plays a key role in astrocyte differentiation during CNS development. We have therefore investigated the early stages of brain and retina development and we have taken advantage of neural progenitor cells (NSCs) derived from striata of embryonic day 14 (E14) as a simplified in vitro model of astrocyte differentiation (Duval et al., 2002; Reynolds & Weiss, 1996; Von Visger et al., 1994). We here report that a progressive increase in AQP4 expression level and the consequent assembly into growing OAPs characterizes astrocytes during their early postnatal development and their differentiation. As a

consequence, astrocytes improve their water transport and migration properties. Furthermore, we show that TRPV4 expression follows an opposite expression pattern, being progressively downregulated during early CNS development and astrocyte differentiation and that its functionality is greatly dependent on AQP4 expression given that intracellular Ca^{2+} dynamics mediated by TRPV4 are profoundly affected by the temporal expression profile of AQP expression levels.

2 | MATERIALS AND METHODS

2.1 | Mice

Experiments were performed in accordance with the European directive on animal use for research and the Italian law on animal care (Italian Health Department Approved Project n 710/2017-PR). Mice and rats were kept under a 12 h dark-to-light cycle, constant room temperature and humidity (22 ± 2°C, 75%), with food and water ad libitum, and supplied with environmental enrichment materials, such as toys and shelters. All experiments were designed to minimize the number of animals used and their suffering. CD1 wild-type (WT) and AQP4 knock-out (KO) mice, and Wistar rats from postnatal day 7 (P7), P14, P21, and 4 months (adult) were used. For protein sample preparation, eight rats or mice, both WT and AQP4 KO were examined at each of the specified time points. For immunofluorescence analysis, four adult (4 M) WT and AQP4 KO mice were used.

2.2 | Antibodies

The following primary antibodies were used: goat polyclonal anti-AQP4 (Santa Cruz, Dallas, TX, USA) diluted to 1:500 for immunoblot and immunofluorescence analyses; mouse monoclonal anti-GFAP (clone G-A-5, Millipore, Burlington, MA, USA) at 1:500 for immunoblot and immunofluorescence; rabbit polyclonal anti-TRPV4 (Alomone, Jerusalem, Israel) at 1:200 for immunoblot and immunofluorescence; rabbit polyclonal anti-Nestin (Sigma-Aldrich, Saint Louis, MO, USA) at 1:1000 for immunoblot and 1:500 for immunofluorescence; mouse monoclonal anti-GS (clone GS-6, Millipore, Burlington, MA, USA). The following secondary antibodies (all from Invitrogen, Waltham, MA, USA) were used for immunofluorescence at dilution of 1:1000: donkey anti-goat Alexa Fluor594, donkey anti-rabbit Alexa Fluor488, donkey anti-mouse Alexa Fluor488, donkey anti-rabbit Alexa Fluor647, donkey anti-mouse Alexa Fluor647. The following secondary antibodies (all from Santa Cruz, Dallas, TX, USA) were used for Western blot diluted to 1:5000: goat anti-mouse IgG-horse- radish peroxidase (HRP); goat anti-rabbit IgG-HRP; donkey anti-goat IgG-HRP.

2.3 | Brain and retina isolation and protein sample preparation

Brain and eyes were harvested from Wistar rats, CD1 WT, and AQP4 KO mice and immediately dissected in ice-cold PBS. After the removal of excessive liquid, the brain and retina were snap-frozen in liquid nitrogen and stored at −80°C. Proteins were extracted from stored explanted brain and retina in 7–10 volumes of RIPA buffer (10 mM Tris HCl, pH 7.4; 140 mM NaCl; 1% Triton X-100; 1% Na deoxycholate; 0.1% SDS; 1 mM Na_3VO4; 1 mM NaF and 1 mM EDTA) added with a cocktail of protease inhibitors (Roche, Indianapolis, IN, USA). The lysis was performed on ice for 1 h and the samples were then centrifuged at 21,000*g* for 1 h. The protein content of the supernatant was measured with a bicinchoninic acid (BCA) Protein Assay Kit.

2.4 | SDS-PAGE and Western blot analysis

30 µg protein samples were separated by NuPAGE 4%–12% Bis-Tris Gel (Invitrogen, Waltham, MA, USA) or 8%, 10%, 12% SDS/PAGE gel and transferred to polyvinylidene difluoride membranes (Millipore, Burlington, MA, USA), as described previously (de Bellis et al., 2021). Membranes with blotted proteins were incubated with primary antibodies, washed, and incubated with peroxidase-conjugated secondary antibodies (Nicchia et al., 2016). Reactive proteins were revealed using an enhanced chemiluminescent detection system (ECL Plus, Thermo Scientific, Rockford, IL, USA) and visualized on a Versadoc imaging system (BioRad, Hercules, CA, USA). Protein levels were expressed as the ratio of densitometric value to whole proteins in Coomassie blue–stained membranes. Densitometry analysis was performed using ImageJ Software (National Institute of Mental Health, Bethesda, Maryland, USA) or Image Lab (BioRad, Hercules, CA, USA) and analyzed by GraphPad Prism 7 (GraphPad, San Diego, CA, USA).

2.5 | Neurosphere culture preparation

Primary cultures of neurospheres were prepared from WT and AQP4 KO mice, as previously described (Duval et al., 2002; Scemes et al., 2003) with minor modifications. Briefly, neural progenitor cells were isolated from the forebrain tissue of 14-day-old (E14) mouse embryos and mechanically dissociated into single cells in ice-cold Phosphate Buffered Saline (PBS Ca^{2+} and Mg^{2+}- free). Cells were centrifuged at 500*g* × 5 min, the supernatant discarded, and the pellet well resuspended in Dulbecco Modified Eagle Medium Nutrient Mixture F12 (DMEM-F12) supplemented with 5% B27, 1% penicillin/streptomycin and 20 ng/mL recombinant epidermal growth factor (EGF). The cell suspension was transferred into tissue culture dishes and allowed to grow into floating neurospheres at 37°C in a humidified atmosphere of 95% O_2 and 5% CO_2. After 48 h, cells were transferred into new tissue culture dishes to remove non-specific adherent cells. Subsequently, fresh EGF was added every 2 days, and two-thirds of the culture medium was replaced twice a week. Neurospheres were passed once a week. Differently from the method described by Duval (Duval et al., 2002) and Scemes (Scemes et al., 2003), neural stem cell subculture was optimized by dissociating neurospheres with Accutase Cell Dissociation Reagent (Thermo, Waltham, MA, USA) for 15 min at room temperature (RT), followed by

addition of the culture medium to halt enzymatic activity. The use of Accutase reagent enhances the dissociation of neurospheres into single cells and promotes neurosphere reformation, as evidenced by previous studies (Diana et al., 2021; Gonmanee et al., 2021; Panchision et al., 2007). Each neurosphere preparation was cultured for a maximum of 1 month, equivalent to four cell passages. Transferring floating neurospheres to an adhesive substrate and removing EGF from standard medium allowed neural progenitors to differentiate. Single neurospheres were plated on glass coverslips, 12- and 96-well plates coated with poly-D-lysine (10 µg/mL) and fibronectin (10 µg/mL) and used as requested.

The specific experimental strategy for experiments on NSCs was chosen depending on the type of experiments. For Western blot and 2D BN/SDS PAGE, NSCs were analyzed until 30 days of differentiation (D30) when neurospheres were almost completely flattened. For immunofluorescence analysis, NSCs were analyzed up to 2 weeks of differentiation when it was possible to distinguish the central core of the neurosphere from the outgrowing layers formed by the migrating cells. Water transport measurements, typically conducted under subconfluent conditions, were also conducted for up to 2 weeks. Progenitor cell migration from the neurospheres was monitored for up to 3 days aligning with studies conducted by Scemes et al. (Scemes et al., 2003) and Striedinger (Striedinger et al., 2007; Striedinger & Scemes, 2008). In the case of calcium imaging, experiments were conducted over a period of up to 3 weeks based on previous studies on calcium imaging in NSCs (Scemes et al., 2003).

2.6 | Native protein sample preparation from retina and neurospheres

Retina and neurospheres were dissolved in three volumes of blue native (BN) buffer (10% glycerol, 500 mM 6-aminohexanoic acid, 1% Triton X-100, 12 mM NaCl, 2 mM EDTA, 20 mM Bis-Tris pH 7.0) added with Protease Inhibitor Cocktail (Roche, Indianapolis, IN, USA). After 1 h incubation on ice, the samples were then centrifuged at 21,000*g* for 30 min at 4°C. The supernatants were collected, and the total protein content was evaluated using the BCA Protein Assay Kit (Thermo, Waltham, MA, USA).

2.7 | BN-PAGE and BN/SDS-PAGE

30 µg protein samples were mixed with 5% Coomassie Blue-250 and loaded onto a polyacrylamide native gradient gel (3%–9%) (Schaägger et al., 1994). Electrophoresis was conducted as described previously (de Bellis et al., 2021). Briefly, the running buffers were as follows: blue cathode buffer (50 mM tricine, 7.5 mM, imidazole, 0.02% Coomassie Blue G-250, pH 7) and anode buffer (25 mM imidazole, pH 7). Electrophoresis was conducted at 6 mA and stopped when the tracking line of the Coomassie Blue G-250 dye had left the edge of the gel. Proteins were transferred onto PVDF membranes (Millipore, Burlington, MA, USA) for immunoblot analysis. Alternatively, the lanes were used for the two-dimensional analysis (2D). For the 2D BN/SDS-PAGE analysis, lanes from the first dimension were isolated into individual strips and equilibrated in denaturing buffer (1% SDS and 1% ß-mercaptoethanol) for 1 h at RT and positioned on the top of a 13% 2D SDS-polyacrylamide gel with the same thickness. After the run, proteins were transferred onto a PVDF membrane (Millipore, Burlington, MA, USA) for Western blot analysis, performed as described above.

2.8 | Immunofluorescence on retina sections and neurospheres

For retina section preparation, eyes were explanted in ice-cold PBS, washed several times, and fixed in 4% PFA solution for 2–3 h at 4°C. After removal of cornea, iris, and lens, whole posterior eyecups were immersed in 30% sucrose solution in PBS overnight; then, eyecups were embedded in OCT compound (Leica Biosystem, Nussloch, Germany) and immediately frozen at −80°C. Sections of 10 µm thickness were cut on a cryostat (CM 1900; Leica) at −20°C. After blocking (2% BSA in PBS), sections were incubated with primary antibodies overnight at 4°C or for 2 h at room temperature in blocking solution, washed for 30 min, and then incubated with secondary antibodies for 1 h. Finally, the sections were washed for 15 min in PBS and mounted with mowiol or in PBS-glycerol (1:1) pH 8.0, containing 1% n-propyl gallate. Immunofluorescence on neurospheres was performed as follows: adherent cultured neurospheres were washed in Ca^{2+}/Mg^{2+} PBS and fixed in 4% PFA for 1 h. After three washes with Ca^{2+}/Mg^{2+} PBS, the neurospheres were permeabilized for 30 min with 0.4% Triton X-100 and incubated with primary antibody for 48 h at 4°C after blocking with 1% BSA in PBS for 1 h. Secondary antibodies were added to the cells for 24 h at 4°C. Coverslips were mounted in PBS-glycerol (1:1) pH 8.0, containing 1% n-propyl gallate.

2.9 | Confocal microscopy and fluorescence analysis

Confocal images were obtained with an automated inverted Leica TCS SP8 confocal microscope using a ×20 and ×40 HC PL Apo oil CS2 objective and Leica LASX software used for image acquisition and analysis (Leica Microsystems CMS GmbH). Excitation of the Alexa Fluor488, 594, and 647 fluorophores was achieved with 488, 591, and 647 nm laser beams. To assess the degree of expression of AQP4, TRPV4, and GFAP images were acquired randomly from each coverslip. Regions of interest (ROIs) were placed on the TRPV4 channel after splitting the three merged channels (488, 594, and 647 nm) and the measurement tool in Fiji was used to analyze the molecular distribution and fluorescence intensity. For that, single-plane confocal images were converted to monochrome (8-bit) images, thresholded, and particles outlined. All fluorescence values are corrected for background contribution. For each neurosphere, three background measurements were taken surrounding the neurosphere. Those measurements were

averaged for use in future calculations. Line scans were drawn from the core of the neurosphere through the migration cells, over the entire ROI, starting ~100 μm inside the core of the neurospheres. Next, the 8-bit grayscale intensity values of the intended markers were measured and used to form a graph.

2.10 | Fluorescence quenching water transport assay

Water transport properties in adherent neurospheres were analyzed by calcein-quenching fluorescence assay, as described previously (Mola et al., 2009, 2021). 15 neurospheres/well were seeded on black, clear bottom 96-well plates (Corning, New York, NY, USA) coated with poly-D-lysine and fibronectin and cultured for 3, 7, and 14 days. Fluorescence signal kinetics in calcein-loaded glial cells after hypotonic or hypertonic gradient were recorded on a Flex Station3 plate reader (Molecular Devices, San Jose, USA) equipped with an integrated automatic liquid handling module. Calcein fluorescence was continuously read for 20 s to establish the baseline signal, representing cell volume under isotonic conditions, and for 100 s after automated addition of an appropriate volume of hypo (water) or hypertonic (D-mannitol 0.5 M) solution in order to obtain 240 mOsm/L or 360 mOsm/L final extracellular osmolarity, respectively. Mannitol was used to maintain the ionic strength of the extracellular solution (Jo et al., 2015; Toft-Bertelsen et al., 2018). There were no further modifications to the external solution, maintaining the cells in an anisotonic medium throughout the recording period. The magnitude of the osmotic gradient applied to the cells is consistent with the common approach for measuring biophysical parameters defining membrane water permeability (Heo et al., 2008; Jo et al., 2015; Solenov et al., 2004). Data acquisition was performed using SoftMax Pro software, and the data were analyzed with Prism software (GraphPad, San Diego, CA, USA). The time constant (τ, s) of cell volume change upon the osmotic stimulus was obtained by fitting the data with an exponential function.

2.11 | Migration index

To determine the contribution of AQP4 during the migration of neural progenitors, floating WT and AQP4 KO NSCs of similar diameters were plated on coated glass-bottom microwells containing DMEM-F12 supplemented with B27 but without EGF. The migration index (Mi) of migrating cells was evaluated as the ratio of the distance of the farther cells to the center of the sphere and the diameter of the sphere core.

2.12 | Calcium imaging and data analysis

For calcium imaging the saline bath was composed of (mM): 140 NaCl, 4 KCl, 2 $MgCl_2$, 2 $CaCl_2$, 10 HEPES, 5 glucose, pH 7.4 with NaOH and osmolarity adjusted to ~318 mOsm with mannitol. Stock solutions of 4alpha-phorbol-12,13-didecanoate (4alpha-PDD, 4αPDD) were prepared by dissolving it in DMSO and kept at −20°C. Changes in intracellular Ca^{2+} concentration ($[Ca^{2+}]i$) were monitored by calcium imaging using the single-wavelengths Ca^{2+} indicator Fluo-4-AM (Life Technologies, Carlsbad, CA, USA). NSCs plated on glass coated with poly-D-lysine were incubated at room temperature for 30 min with Fluo-4-AM (1 μM) dissolved in the standard external solution. Experiments were performed 3, 7, 14, and 21 days after NSC plating. Measurements of $[Ca^{2+}]i$ were performed by using a high-resolution upright confocal spinning disk microscope (Fluo Spin up, Crisel Instruments, Rome) equipped with a water immersion objective (×40, Olympus) and appropriate filters. The excitation wavelength was 470 nm, filtered from a broadband LED light source. Light pulse durations were set to 200 ms, starting 30 s from the beginning of the experiment, while camera exposure times were set to 100 ms with a sampling rate of 2 Hz. Data acquisition was controlled by Metamorph software (Molecular Devices, Sunnyvale, CA, USA).

Regions of Interest were defined, and relative data were extracted using Metamorph. The ratio between the intensity of the fluorescence collected at each time point (Ft) and the initial fluorescence (Ft0), defined as ΔF/F, directly correlates with the variation of intracellular calcium concentration ($[Ca^{2+}]i$). Extracted data were imported for analysis in Origin 8.5, where raw fluorescence traces were normalized and processed to extract different calcium response metrics. Alignment of traces relative to Ca^{2+} delivery was performed by locating the peak for fluorescence intensity as a function of time for each imaging experiment's average time series. Time series data for each cell was subsequently truncated to the first 5 s for analysis purposes. Each cell's raw fluorescence intensity was normalized with respect to the mean raw intensity of the 10 frames, which are reported and analyzed as fractions (dF/F).

2.13 | Statistical analyses

Mean ± standard error (SEM) is reported in the results. For the comparison of the two groups, we used a Student's *t* test, and the statistically significant difference was reported as follows: $*p < .05$, $**p < .01$, $***p < .001$, and $****p < .0001$. When comparing three or more groups we used a one-way analysis of variance (ANOVA) with pair-wise post hoc Tukey's and Newman–Keuls multiple comparison test and a two-way ANOVA with Bonferroni's post hoc test. Within each genotype, different letters on top of each bar indicate significant difference ($p < .05$) between them, and equal letters indicate no significant difference. When statistical analysis was conducted at multiple levels in the same graph, different letters on top of each bar were used to indicate significant differences within the same genotype in terms of analyzed time points or experimental conditions, while asterisks were used to indicate significant differences between the two groups of different genotypes. The specific test used, and the number of experiments (*n*) are indicated in the text or the figure legends. The results reported are the mean of at least three different experimental trials performed in triplicate or more. Statistical analysis was performed using GraphPad

Prism 7 (GraphPad, San Diego, CA, USA) and Origin 8.5 software (Northampton, MA, USA).

3 | RESULTS

3.1 | The water channel AQP4 and the calcium-permeable channel TRPV4 are differentially regulated during postnatal development in the brain and retina of rat and mouse

The temporal expression profile of the protein channels AQP4 and TRPV4 during brain and retina postnatal development was first examined by Western blotting using astrocyte and Müller cells markers GFAP and glutamine synthetase (GS), respectively, in rat and wild-type (WT) mouse tissues (Figure 1a–d, Table 1). A similar trend for AQP4 and GFAP in the brain (Figure 1a,b) and for AQP4 and GS in the retina (Figure 1c,d) was found in rat and mouse, with AQP4 and the glial markers progressively increasing from postnatal day 7 (P7) to 4 month-old (4 M) adult. While in the brain the expression levels of both AQP4 and the glial marker were already detectable at P7 and progressively increased from P7 to 4 M, in the retina their expression appeared delayed. In particular, in rat retina, AQP4 expression at P7 and P14 was 0.98 ± 0.1% and 1.15 ± 0.1%, respectively, in percentage of adult levels ± SEM. A further increase occurred at P21 when the expression levels amounted to 13.11 ± 0.8% of levels in the adult retina. Likewise in the mouse retina, AQP4 exhibited low expression at P7 and P14 (0.1 ± 0.01% and 2.9 ± 0.3%, respectively, in percentage of adult levels ± SEM), with a further increase to 57.7 ± 3.2% at P21. The parallel analysis of GS showed very low expression at P7 in both rat and mouse retina (0.14 ± 0.1% and 0.8 ± 0.1%, respectively, in the percentage of adult levels ± SEM), with an important increase at P14 (52.02 ± 6.7% and 46.5 ± 3.9%, respectively) and P21 when it almost reached its adult levels in both rat and mouse retina with 92.54 ± 9.9% and 93.18 ± 2.7%, respectively. The temporal expression profile of the TRPV4 channel, investigated in parallel, showed important differences in the trend. For rat TRPV4, a decreasing temporal expression pattern was found in both the brain and retina. TRPV4 peaked at P7 (226.3 ± 15.8% and 199.9 ± 9.6%, respectively, in percentage of adult levels ± SEM) and gradually decreased at P14 (141.6 ± 7.5% and 117.8 ± 9.8%, respectively) and P21 (116.9 ± 6.8% and 99.87 ± 3.5%, respectively; Figure 1a,c). Similarly, TRPV4 exhibited high expression at P7 in both mouse brain and retina (561.2 ± 24.9% and 337 ± 26.9%, respectively), with a further decrease at P14 (235.3 ± 13.8% and 190.5 ± 18.7%, respectively) and P21 (133.5 ± 9.8% and 136.1 ± 6.8%, respectively, in percentage of adult levels ± SEM). Altogether, these data indicate that water and calcium homeostasis is finely tuned by AQP4 and TRPV4 synchronized regulation during postnatal CNS development and, in particular, that: (a) AQP4 expression correlates with glial differentiation markers and progressively increases during brain and retina postnatal development; (b) the expression of AQP4 and the glial markers is 2 weeks delayed in the retina compared to the brain; (c) TRPV4 expression follows an opposite trend with a peak at P7 and no major differences between brain and retina.

3.2 | AQP4 deletion differentially affects TRPV4 channel expression levels in brain and retinal glial cells

The widely reported functional relationship between AQP4 and TRPV4 (Benfenati et al., 2011; Jo et al., 2015; Mola et al., 2016) prompted us to analyze whether the selective ablation of AQP4 channel affects TRPV4 expression during postnatal development. We took advantage of AQP4 knock-out (KO) mice in which the trend of TRPV4, GFAP, and GS regulation during brain and retina postnatal development was found to be similar to the WT (Figure 1e,f; Table 2).

The temporal expression profile of TRPV4 expression in WT and AQP4 KO mouse brain and retina was first evaluated by Western blot (Figure 2a,b). Western blotting analysis revealed no differences in TRPV4 expression between WT and AQP4 KO mice in the brain (Figure 2a). In contrast, differences in TRPV4 expression between WT and AQP4 KO were found in the retina (Figure 2b) with TRPV4 expression strongly downregulated in AQP4 KO compared with WT at all the time points analyzed except P7 (Table 3). The western blot analysis of the Müller cell marker GS revealed comparable GS expression levels between WT and AQP4 KO retinas at all time points analyzed, indicating the absence of a major impact of AQP4 deletion on retinal Müller cells (Figure S1). The altered expression of TRPV4 observed in AQP4 KO mouse retinas was then investigated by immunofluorescence (Figure 2c). Single-slice confocal images showed, in line with previous studies, that in the adult WT retina the AQP4 immunostaining was very strong and localized mostly along the vitreal surface and on endfeet membranes of Müller cells facing the retinal capillaries (Nagelhus et al., 1998). Here, TRPV4 was found to be mainly expressed by retinal ganglion cells and Müller cells (Ryskamp et al., 2011) and in co-localization with AQP4 at the endfeet forming the pericapillary sheet in the ganglion cell layer (GCL) and radial processes traversing the inner plexiform layer (IPL) and outer nuclear layer (ONL) of Müller cells. On the other hand, the parallel analysis performed in AQP4 KO mouse retina revealed downregulation of TRPV4 in the Müller cell processes spanning the inner nuclear layer (INL), outer plexiform layer (OPL), and ONL. These results indicate that AQP4 deletion massively affects TRPV4 expression in Müller cells in the retina while leaving its levels unaltered in the brain.

3.3 | AQP4 expression increases during neuronal stem cell differentiation into astrocytes

The observed synchronized regulation of AQP4 and TRPV4 during CNS postnatal development (Figure 1) and the effect of AQP4 deletion on TRPV4 expression (Figure 2) prompted us to analyze such phenomenon in astrocyte differentiation using the neuronal stem cell (NSC) model (Figure 3). In the presence of EGF, NSCs grow as floating neurospheres, while in the absence of EGF and on PDL and

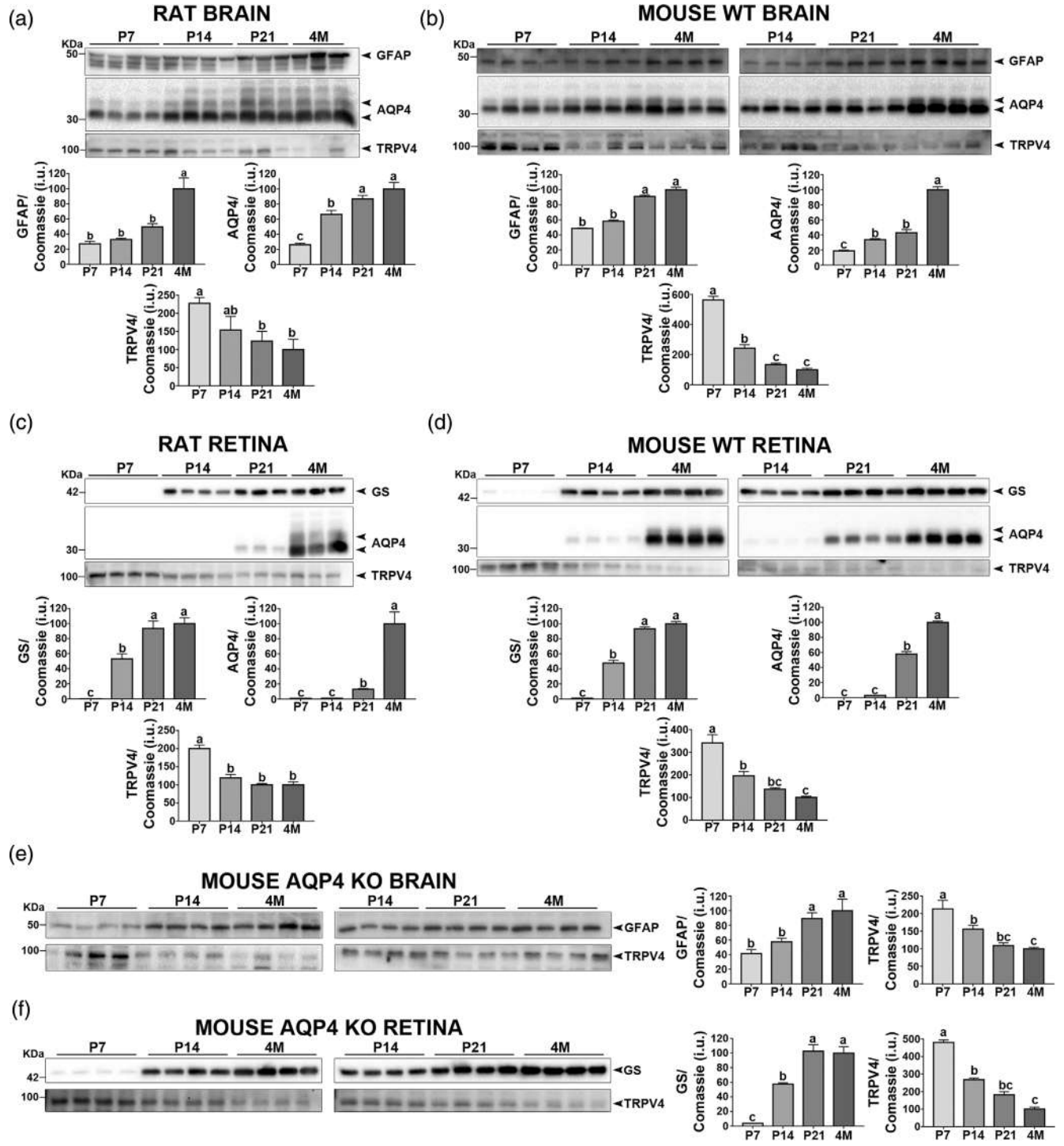

FIGURE 1 Western blot analysis of GFAP, AQP4, and TRPV4 expression in developing rat and mouse brain and retina. (a, b) Representative Western blots and corresponding densitometric analysis showing the expression of the glial cell marker GFAP, AQP4, and TRPV4 in developing (P7–P21) and 4 month-old adult (4 M) rat (a) and WT mouse (b) brain, as indicated. (c, d) Representative Western blots and corresponding densitometric analysis showing the expression of the Müller cell marker glutamine synthetase (GS), AQP4 and TRPV4 in developing (P7–P21) and 4 month-old adult (4 M) rat (c) and WT mouse (d) retina. (a–d) Data (summarized in Table 1) are expressed as means of intensity unit (i.u.) ± SEM. (e) Representative Western blots and corresponding densitometric analysis showing the expression of the glial cell marker GFAP and TRPV4 in developing (P7–P21) and 4 month-old adult (4 M) AQP4 KO brain. (f) Representative Western blots and corresponding densitometric analysis showing the expression of the Müller cell marker glutamine synthetase (GS) and TRPV4 in developing (P7–P21) and 4 month-old adult (4 M) AQP4 KO retina. Data (summarized in Table 2) are expressed as means of intensity unit (i.u.) ± SEM. Coomassie blue-stained PVDF membrane was used as a loading control. Different letters indicate a significant difference at $p < .05$ determined by One-way Anova and Tukey's Multiple Comparisons Test ($n = 8$). Arrowheads indicate the bands recognized by the antibodies at the expected molecular weight. Molecular-mass markers (in kDa) are shown on the left of each blot.

TABLE 1 Densitometry values of GFAP, GS, AQP4, and TRPV4 protein expression levels at P7, P14, and P21 expressed as a percentage relative to that of the adult (4 M), considered as 100%. Data are expressed as mean ± SEM, $n = 8$ in each group.

		Rat				WT mouse			
		P7	P14	P21	4 M	P7	P14	P21	4 M
Glial Marker	Brain (GFAP)	26.17 ± 3.5	32.45 ± 1.9	48.89 ± 4.4	100 ± 4.5	48.47 ± 0.7	57.97 ± 1.8	90.95 ± 1.7	100 ± 3.4
	Retina (GS)	0.14 ± 0.1	52.02 ± 6.7	92.54 ± 9.9	100 ± 7.7	0.8 ± 0.1	46.5 ± 3.9	93.18 ± 2.7	100 ± 2.8
AQP4	Brain	25.78 ± 2.1	65.66 ± 5.3	86.81 ± 4.5	100 ± 8.8	18.54 ± 1.3	33.53 ± 1.3	41.89 ± 4.4	100 ± 3.9
	Retina	0.98 ± 0.1	1.15 ± 0.1	13.11 ± 0.8	100 ± 5.6	0.1 ± 0.01	2.94 ± 0.3	57.73 ± 3.2	100 ± 1.9
TRPV4	Brain	226.3 ± 15.8	141.6 ± 7.5	116.9 ± 6.8	100 ± 8.6	561.2 ± 24.9	235.3 ± 13.8	133.5 ± 9.8	100 ± 7.1
	Retina	199.9 ± 9.6	117.8 ± 9.8	99.87 ± 3.5	100 ± 8.5	337 ± 26.9	190.5 ± 18.7	136.1 ± 6.8	100 ± 5.9

TABLE 2 Densitometry values of GFAP, GS, and TRPV4 protein expression levels shown in AQP4 KO mouse brain and retina in Figure 1e,f. Protein abundance is expressed as the percentage relative to that of the adult (4 M), considered as 100%. Data are expressed as mean ± SEM, $n = 8$ in each group.

AQP4 KO mouse		P7	P14	P21	4 M
Glial Marker	Brain (GFAP)	38.57 ± 5.5	55.27 ± 5.2	89.45 ± 7.7	100 ± 15.8
	Retina (GS)	3.852 ± 0.2199	57.44 ± 1.77	101.3 ± 9.248	100 ± 8.851
TRPV4	Brain	209.4 ± 24.9	153.9 ± 10.5	108.4 ± 7.9	100 ± 4.1
	Retina	480.2 ± 14.3	266.8 ± 9.6	179.5 ± 7.7	100 ± 8.2

fibronectin-coated surfaces they progressively form a monolayer of astrocytes (Figure 3b). In the present study, NSCs were induced to differentiate for 30 days by removing EGF and analyzed in terms of morphology and expression levels of glial and staminal markers after 4 h 7, 15, and 30 days (Figure 3a). The analysis of mouse floating neurospheres by confocal microscopy (Figure 3c), using GFAP as a marker of glial progenitors and the intermediate filament protein Nestin as a marker of undifferentiated neural progenitors, revealed that the neurospheres are made of a mixed population of both cell types, as expected (Reynolds & Weiss, 1996). AQP4 staining was detected predominantly in GFAP-positive glial progenitors at the periphery of undifferentiated neurospheres. GFAP, Nestin, and AQP4 were later analyzed by Western blotting in differentiating NSCs prepared from mice and rats (Figure 3d). The results show that Nestin expression progressively decreased, while GFAP and AQP4 levels increased during NSC differentiation into the astrocyte lineage. Altogether these results indicate that: (a) AQP4 is expressed in GFAP-positive glial progenitors and not in Nestin-positive neural progenitors; (b) astrocyte differentiation is associated with increasing AQP4 expression both in mouse and in rat NSCs; and (c) NSCs can be considered a valuable model to study the role of AQP4 during astrocyte differentiation.

3.4 | AQP4 aggregation into supramolecular assemblies occurs during CNS postnatal development and astrocyte differentiation

The AQP4 plasma membrane feature of adult differentiated astrocytes in the CNS consists of its supramolecular level of aggregation into assemblies known as Orthogonal Arrays of Particles (OAPs). We next evaluated whether the AQP4 progressive increase associated with postnatal CNS development (Figure 1) and astrocytes differentiation (Figure 3) was accompanied by modification in the AQP4 aggregation state within the AQP4 assemblies (Figure 4). Two-dimensional electrophoresis (Nicchia et al., 2008; Sorbo et al., 2008) was used to analyze membrane proteins extracted from developing retina and from mouse and rat differentiating NSCs, separated under native conditions on a 3%–9% acrylamide gradient gel BN–PAGE, and then subjected to a denaturing 2D (SDS–PAGE) 13% acrylamide gel. AQP4 immunoblot performed on developing retina (Figure 4a) revealed that the tetrameric form is barely detectable at P14, while the size of AQP4 assemblies progressively increases until the latest stages of differentiation (adult retina) when the majority of AQP4 is expressed as the largest AQP4 aggregate detectable. Similarly, results shown in Figure 4b revealed that the majority of AQP4 is expressed under the tetrameric form in undifferentiated mouse NSCs, while larger AQP4 assemblies are progressively revealed during NSC differentiation into astrocytes. Comparable results were obtained in rat neurospheres, with different-sized AQP4 assemblies already visible in undifferentiated NSCs and larger-sized assemblies progressively increasing during differentiation. These results indicate that: (a) AQP4 supramolecular organization in larger-sized assemblies is a feature of mature astrocytes and Müller cells and likely takes place during their differentiation occurring in CNS postnatal development; (b) the NSC model of differentiation is also able to reproduce the progressive AQP4 supramolecular organization in larger sized assemblies occurring in astrocytes and Müller cells during the first weeks of postnatal development.

3.5 | AQP4-dependent increase in plasma membrane water permeability and migratory capability occurs during NSC differentiation into astrocytes

The water transport properties and the migratory capability conferred by the increasing AQP4 expression and aggregation state observed

during NSC differentiation were investigated using NSCs prepared from WT and AQP4 KO mice (Figure 5). Water transport properties were monitored by calcein quenching assay after 3, 7, and 14 days of differentiation. Measurements conducted up to 14 days were sufficient to highlight the correlation between the temporal increase in AQP4 expression and the rate of cell swelling as well as to confirm the slower swelling of AQP4 KO cells compared to WT. Time courses of cell swelling (Figure 5a) and shrinking (Figure 5b) after hypotonic or hypertonic stimuli recorded in WT NSCs revealed that NSCs progressively accelerate the cell volume change rates during their differentiation into the

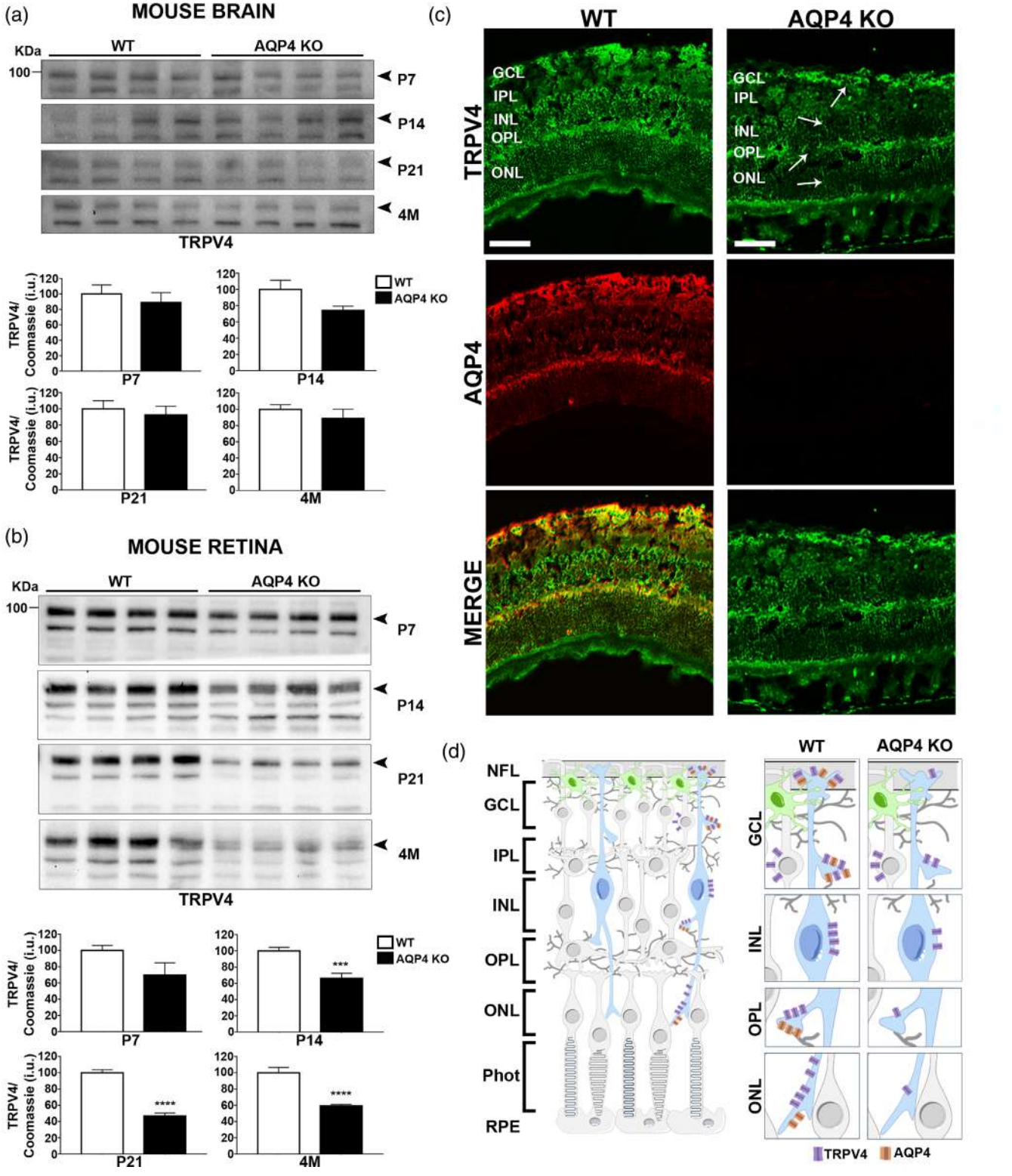

FIGURE 2 Legend on next page.

TABLE 3 Densitometry values of TRPV4 protein expression levels in AQP4 KO brain and retina expressed as a percentage relative to that of age-matched WT, considered as 100%. Data are expressed as mean ± SEM, $n = 8$ in each group.

		P7	P14	P21	4 M
TRPV4	AQP4 KO Brain	86.60 ± 8.5	74.21 ± 5.2	92.58 ± 10.7	88,87 ± 9.8
	AQP4 KO Retina	69.66 ± 15.2	66.24 ± 6.2	46.76 ± 3.7	59.22 ± 1.8

glial lineage. As expected, the analysis of both swelling and shrinking phases of AQP4 KO NSCs revealed significantly slower time constant values compared to WT and did not show any variations during the time points of differentiation here analyzed.

Based on the established role of AQP4 in sustaining astrocyte migration (Saadoun et al., 2005; Smith et al., 2014), the migratory behavior of WT and AQP4 KO NSCs during differentiation into astrocytes was later analyzed (Figure 5c). NSCs with similar diameters were plated on coated glass-bottom microwells and the distance of migration of neural progenitors out of the neurosphere was then analyzed after 3 h and 1, 2, and 3 days, in line with studies performed by Scemes (Scemes et al., 2003) and Striedinger (Striedinger et al., 2007; Striedinger & Scemes, 2008). WT and AQP4 KO NSCs showed a progressive increase in their migration index (Mi) during differentiation into the glial lineage. However, this increase was highly slowed down in AQP4 KO NSCs compared with WT, indicating an important effect of AQP4 deletion on the migratory behavior of NSCs. These data show that astrocyte differentiation is associated with a progressive increase in plasma membrane water permeability and NSC migratory capability.

3.6 | AQP4 opposite TRPV4 expression pattern in differentiating NSCs mirrors that of CNS postnatal development

The coordinated TRPV4 and AQP4 expression during CNS postnatal development (Figure 1) and TRPV4 downregulation in AQP4 KO retina (Figure 2) next prompted us to determine TRPV4 expression in WT and AQP4 KO differentiating NSCs by Western blot and confocal microscopy (Figure 6). In line with results obtained during CNS postnatal development, Western blot analysis showed that TRPV4 expression peaked in both WT and AQP4 KO undifferentiated neurospheres (4 h), and gradually decreased during their differentiation. Additionally, TRPV4 expression was found to be similar between the WT and AQP4 KO at the analyzed time points (Figure 6a). Then we sought to perform the same analysis by confocal microscopy on differentiating NSCs triple-stained for TRPV4, AQP4, and GFAP (Figure 6b,c). In line with Western blotting analysis, TRPV4 expression progressively decreased during NSC differentiation in both WT and AQP4 KO. In contrast, AQP4 was weakly expressed in WT undifferentiated NSCs, whereas no staining was detected in the AQP4 KO, as expected. The analysis performed at 15 days of NSC differentiation showed TRPV4 expression to be concentrated into the center of the neurosphere, whereas only a few TRPV4-positive cells were observed in the outer migrating cells, in both the WT and AQP4 KO. On the contrary, AQP4 expression in the WT and GFAP expression in both the WT and AQP4 KO NSCs were strongly expressed in the spreading outgrowth, whereas they were weakly detectable in the center of the neurospheres. Thus, these results further support the different trends of AQP4 and GFAP versus TRPV4 expression pattern and strongly indicate it to be ascribable to astrocyte differentiation occurring during CNS development.

3.7 | TRPV4 mediated $[Ca^{2+}]_i$ dynamics are finely tuned during astrocyte differentiation and are severely downregulated by AQP4 deletion

The dynamics of $[Ca^{2+}]_i$ in WT and AQP4 KO NSCs were monitored before and after the exposure to 4αPDD (Figure 7a–d, left and right panels), a selective activator of TRPV4 (Benfenati et al., 2007, 2011). Representative traces of calcium imaging experiments performed after 3 days in vitro (D3) demonstrate that basal $[Ca^{2+}]_i$ dynamics in both

FIGURE 2 TRPV4 expression analysis in AQP4 KO brain and retina. Representative Western blots and densitometric analysis showing the temporal expression pattern for TRPV4 in developing (P7–P21) and 4 month-old adult (4 M) WT and AQP4 KO mouse brain (a) and retina (b). TRPV4 expression is only significantly reduced in the retina of AQP4 KO mice. Coomassie blue-stained PVDF membrane was used as a loading control. Data (Table 3) represent means of intensity unit (i.u.) ± SEM. Unpaired Student's *t* test was performed. ***$p < .001$; ****$p < .0001$ ($n = 8$). Arrowheads indicate the bands recognized by the antibodies at the expected molecular weight. Molecular-mass marker (in kDa) is shown on the left of each gel. (c) Single-slice confocal images of adult (4 M) WT and AQP4 KO mouse retina immunostained with AQP4 (red) and TRPV4 (green) antibodies and their merging. Note that TRPV4 immunolabeling is downregulated in Müller cells spanning the NLF/GCL, INL, OPL, and ONL (arrows), as shown in the drawing at the bottom. ($n = 4$) Scale bar 50 µm. (d) Drawing of mouse retina with highlighting in green of astrocytes in the GCL and in blue of the Müller cells spanning from NFL to ONL. TRPV4 and AQP4 are shown in purple and orange, respectively. The intraretinal vasculature is shown in dark gray. Left, the TRPV4 in mouse retina is expressed by ganglion cells, localized at the NFL/GCL interface, and by Müller cells colocalizing with AQP4 at the endfeet forming the pericapillary sheet in the NFL/GCL and radial processes traversing the IPL and ONL. Right, at higher magnification note the TRPV4 downregulation occurring in the Müller cells process spanning the INL, OPL, and ONL. (NFL, Nerve Fiber Layer; GCL, Ganglion Cell Layer; IPL, Inner Plexiform Layer; INL, Inner Nuclear Layer; OPL, Outer Plexiform Layer; ONL, Outer Nuclear Layer; Phot, Photoreceptor layer; RPE, Retinal Pigment Epithelium).

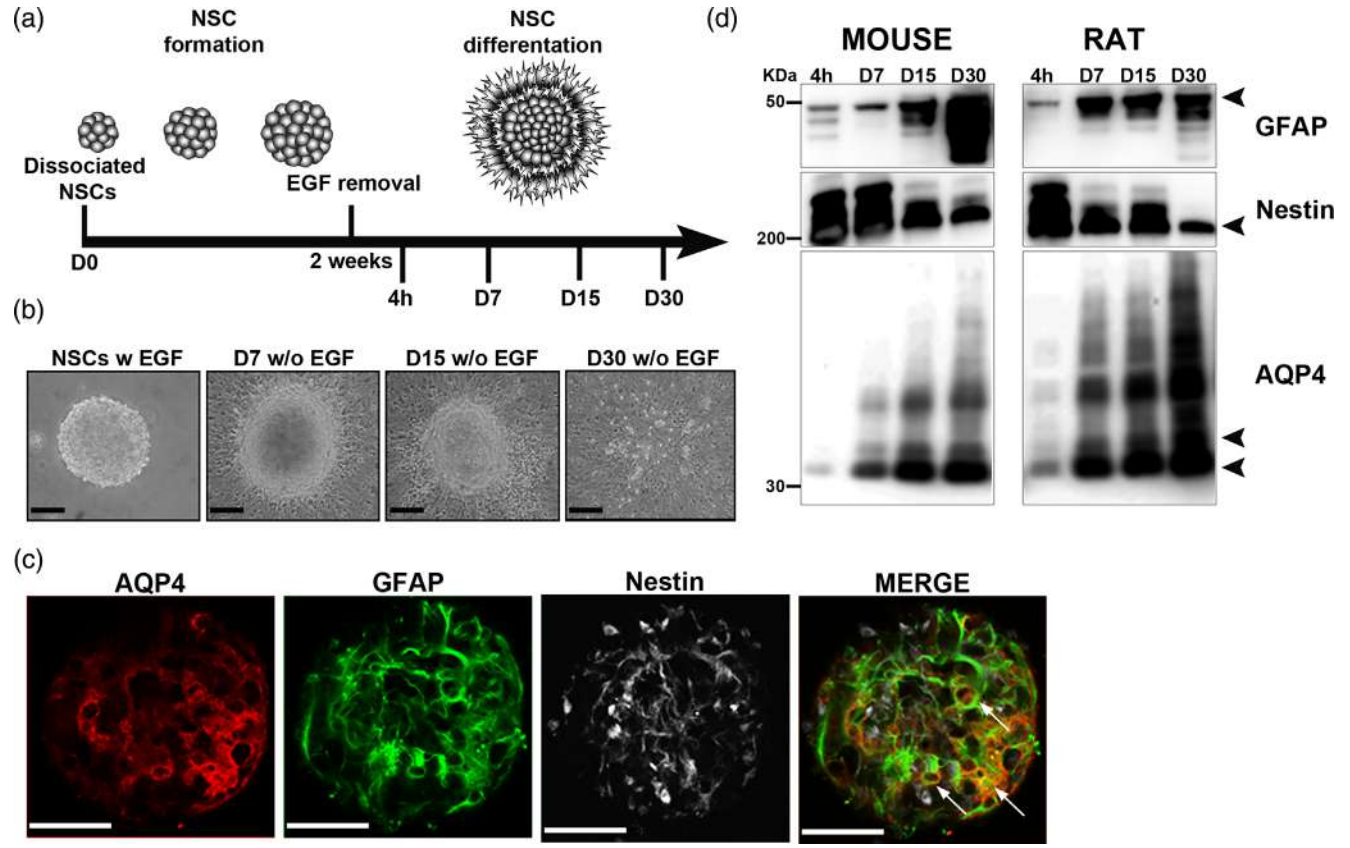

FIGURE 3 Characterization of neural stem cell (NSC) cultures. (a) Image of the time-scale analysis of mouse NSC growth from day 0 (D0) to 2 weeks in the presence of EGF. At 2 weeks, NSC differentiation into astrocytes is induced by EGF removal. NSCs were analyzed after 4 h and 7, 15, and 30 days (D7, D15, and D30, respectively) of differentiation. (b) Phase-contrast micrographs showing the NSCs growing as floating neurospheres in the presence of EGF (w EGF) and during their differentiation into glial lineage in the absence of EGF (w/o EGF) on fibronectin and the poly-D-lysine coated surface. At D7 outgrowing cells formed layers surrounding the neurosphere. From D7 to D30, the number of cells within the neurosphere progressively decreased while it increased in the outgrowth. At D30 the neurospheres were almost completely flattened. Scale bar 50 μm. (c) Confocal microscopy analysis of floating neurospheres immunostained with AQP4 (red), the glial marker GFAP (green), the protein marker for neural progenitor Nestin (white), and their merging. Arrows indicate AQP4 and GFAP colocalization. Scale bar 50 μm. (d) Western blot analysis showing the time course of GFAP, Nestin, and AQP4 expression in differentiating neurospheres prepared from mouse and rat at 4 h, and D7, D15, and D30. Arrowheads indicate the bands recognized by the antibodies at the expected molecular weight. Molecular-mass marker (in kDa) is shown on the left of each gel. Note that the GFAP and AQP4 expression levels increased, whereas Nestin expression decreased in both mouse and rat NSCs.

WT and AQP4 KO cells were stable during the recording. On the other hand, the exposure to 4αPDD induced an oscillatory as well as sustained response in WT NSC (Figure 7a, left panel), but not in AQP4 KO NSC cells (Figure 7a, right panel). After 7 days (D7), spontaneous oscillatory $[Ca^{2+}]_i$ dynamics were detected in NSCs from WT and AQP4 KO NSCs (Figure 7b, left and right panel). Notably, 4αPDD induced a fast and intense increase in oscillatory dynamics in WT cells, whereas the response to the same agonist was absent in NSC from AQP4 KO (Figure 7b, right panel). Similarly, after 14 days (D14), 4αPDD induces an increase in WT cells, (Figure 7c, right panel) while NSCs isolated from AQP4 KO were almost silent before and after the addition of 4αPDD (Figure 7c, right panel). Interestingly, at D21 NSCs from AQP4 KO (Figure 7d, right panel) showed spontaneous oscillatory activity that is not affected after exposure to 4αPDD, while the spontaneous activity in WT cells was very high but not significantly altered in magnitude upon TRPV4 activation (Figure 7d, left panel).

Quantitative analyses of maximum change in relative fluorescence, expressed as ΔFt/Ft0 (Figure 8a) confirmed that WT NSCs displayed spontaneous oscillatory behavior at each time point analyzed (Figure 8a, white bars). Nonetheless, the exposure of 4αPDD induced a massive increase in the magnitude of the oscillations from D3 to D14 with respect to the basal activity (Figure 8a–d, gray bars). Notably, in WT NSC the amplitude of the response to 4αPDD reached its peak at D7 and then it tended to decrease. In contrast, the frequency of the oscillations continued to increase after D3 up to D14 and then remained stable until D21. AQP4 KO NSCs were quiescent from D3 to D7 and then displayed spontaneous activity from D14 to D21 (Figure 8a–d, black bar). Notably, the amplitude of the basal spontaneous oscillations was not significantly altered by the exposure to 4αPDD at D3 and D14 (Figure 8a–d, light gray bar). The magnitude of the $[Ca^{2+}]_i$ was significantly higher, with respect to the basal activity, at D7 and D21. Notably, the frequency of the oscillation observed

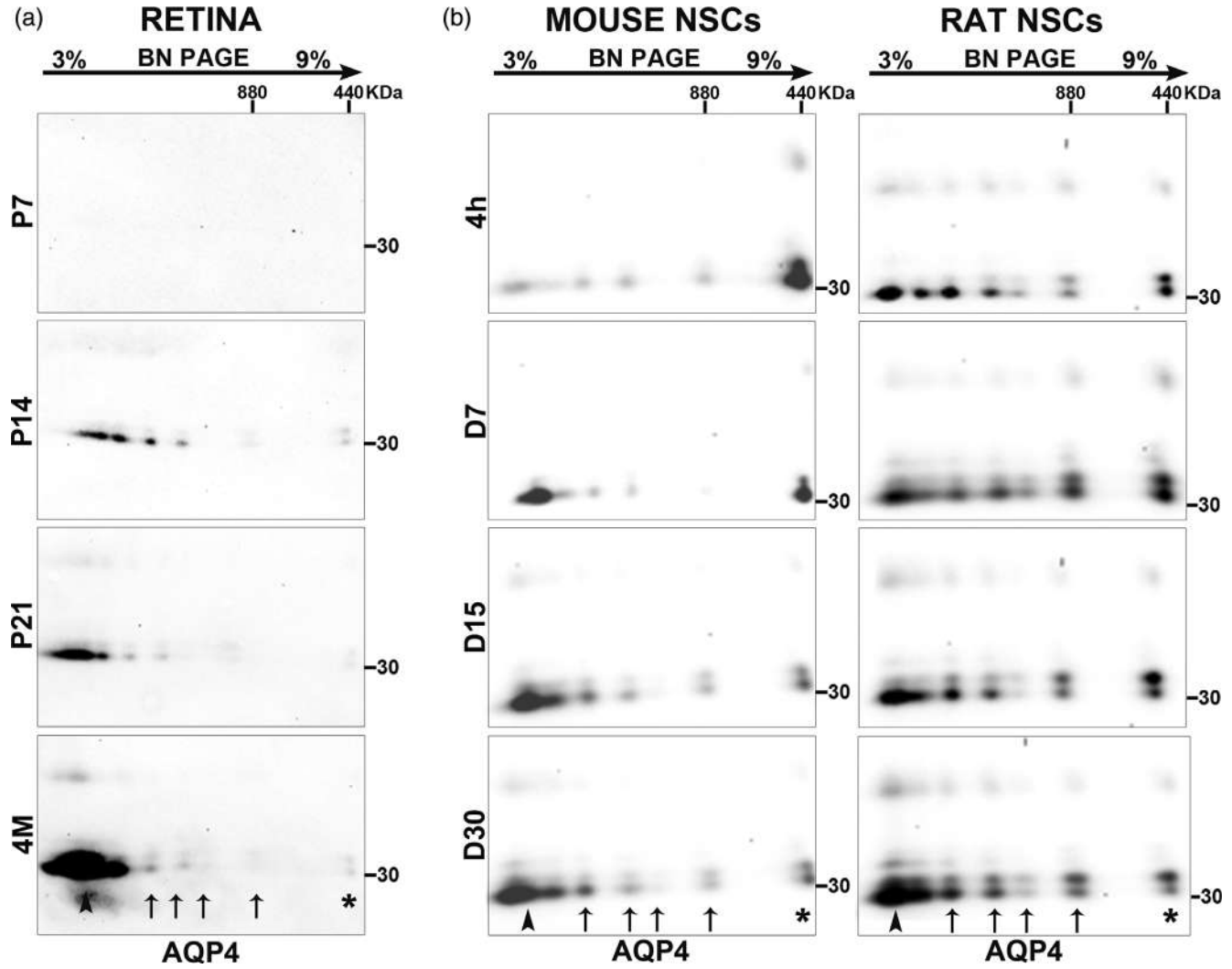

FIGURE 4 BN/SDS-PAGE analysis of AQP4 assemblies during retina postnatal development and NSC differentiation into astrocytes. (a, b) Proteins were separated under native conditions on 3%–9% acrylamide gels (BN-PAGE) and then subjected to 13% SDS-PAGE immunoblot using AQP4 antibodies. AQP4 was detected as the smallest pool at 440 kDa (asterisk), several distinct different sized pools higher than 880 kDa (arrows), and the largest detectable pool (arrowhead). (a) 2D BN/SDS-PAGE AQP4 immunoblot analysis of developing (P7, P14, and P21) and 4 month-old adult (4 M) mouse retina. Note that at P7 no AQP4 was detected while the ratio of progressively larger-sized AQP4 assemblies increased from P14 to 4 M with the majority of AQP4 expressed as the largest resolved aggregate (arrowhead) at 4 M. (b) 2D BN/SDS-PAGE AQP4 immunoblot analysis of mouse and rat differentiating NSCs (4 h, D7, D15, and D30), as indicated. Note that in mouse neurospheres at 4 h, the majority of AQP4 was expressed as tetramers (asterisk). In contrast, the ratio of AQP4 aggregate larger size progressively increased during NSC differentiation with the majority of AQP4 expressed as the largest resolved aggregate (arrowhead) at D30. Comparable results were obtained in rat neurospheres with different medium-sized AQP4 aggregates already visible in undifferentiated neurospheres but with the ratio of larger sized AQP4 aggregates progressively increasing until D30.

upon 4αPDD exposure increased constantly over time reaching its maximum value at D21 (Figure 8d). Figure 8c reports the percentage of responding cells.

4 | DISCUSSION

In the present study, we show that early postnatal neurodevelopment is subjected to temporally modulated water and Ca^{2+} dynamics likely to be those promoting the biomechanical and biophysical changes required for the CNS morphological and functional maturation.

In contrast to the well-characterized role in adult brain homeostasis (Benfenati et al., 2011; Jo et al., 2015; Mola et al., 2016), little is known about AQP4-TRPV4 involvement in neurodevelopment. To such purpose, we investigated the molecular and functional-related properties of these channels across different stages of postnatal development in animal tissues of rats and mice, as well as in animal-derived in vitro cultured NSCs. To dissect the specific contribution of AQP4 to the process, we used AQP4 KO mice. As for the time points, we focused on the first postnatal weeks when the growth of blood vessels and neurogenesis concur with the establishment of the blood–brain barrier and synapse formation, respectively (Bautch &

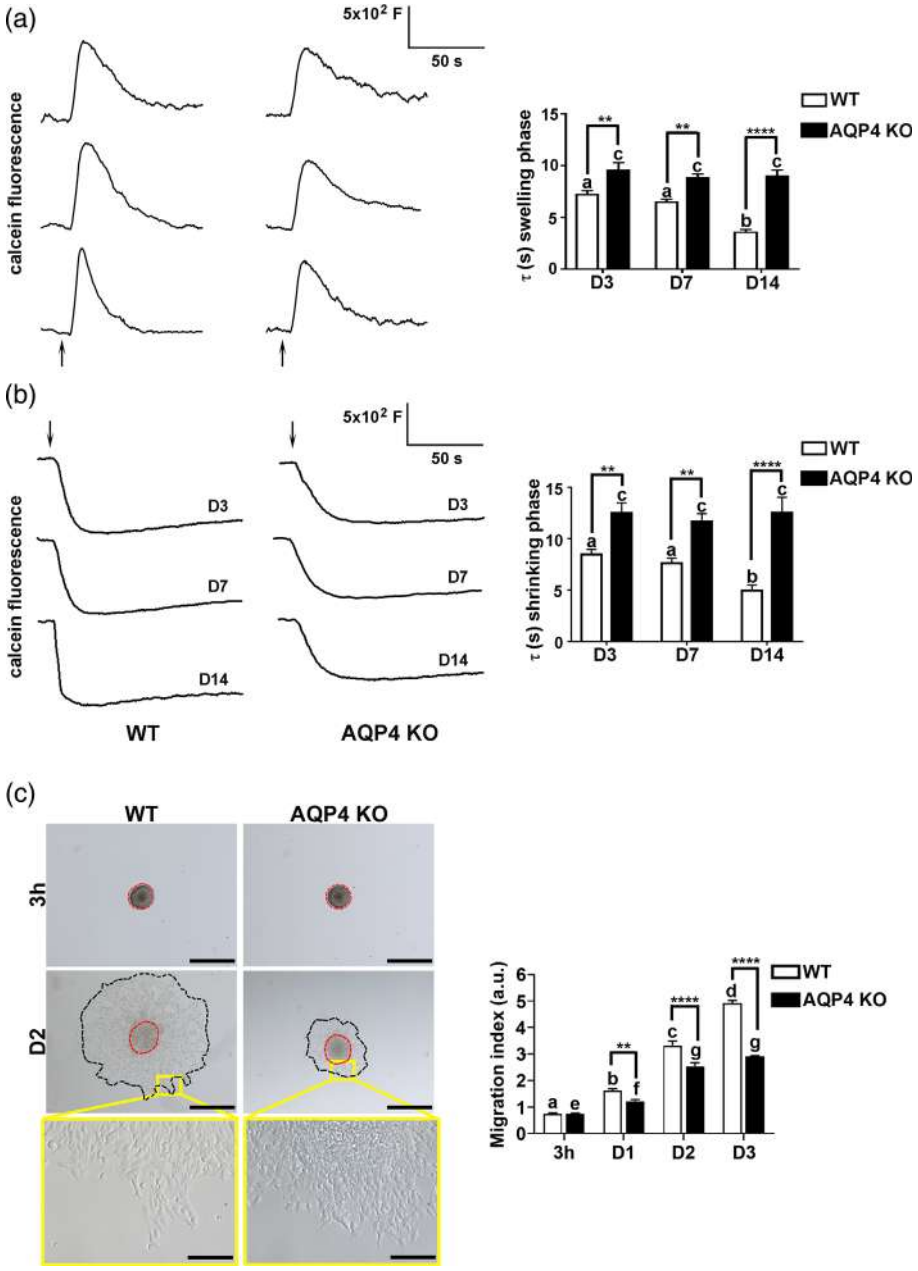

FIGURE 5 Calcein quenching water transport and migration assay of WT and AQP4 KO NSCs during differentiation. (a) Left, representative time courses of cell swelling, recorded for the indicated calcein-AM loaded NSCs, elicited by hypotonic stimulation (240 mOsm/L; Δ 60 mOsm/L) at 3, 7, and 14 days (D3, D7, and D14, respectively) of culture in differentiation conditions. The arrow indicates the switch in the external osmolarity. Right, quantitative analysis of the cell swelling time constants (τ) measured in WT (white bars) and AQP4 KO (black bars) NSCs. (b) Left, representative time courses of cell shrinking, recorded for the indicated calcein-AM loaded NSCs, in response to hypertonic stimulation (360 mOsm/L; Δ 60 mOsm/L) at 3, 7, and 14 days (D3, D7, and D14, respectively) of culture in differentiation conditions. The arrow indicates the switch in the external osmolarity. Right, quantitative analysis of the cell shrinking time constants (τ) measured in WT (white bars) and AQP4 KO (black bars) NSCs. Data represents means ± SEM. A Two-way ANOVA and Bonferroni's Multiple Comparison Test was performed. *$p < .05$; **$p < .01$; ****$p < .0001$. Within each genotype, different letters on top of each bar indicate a significant difference ($p < .05$) between them and equal letters indicate no significant difference ($n = 3$ independent experimental data set). (c) Left, phase-contrast images of the migration of WT and AQP4 KO NSCs after 3 h and 2 days (D2) of culture in differentiation conditions. The red dashed line encloses the NSC core while the black dashed line encloses the outgrowth edge formed by migrating cells. Scale bar 500 μm. Bottom panel: boxed yellow areas are shown at higher magnification highlighting the outgrowth edge formed by migrating cells. Scale bar 100 μm. Right, histogram showing the Migration index (Mi) calculated for WT and AQP4 KO NSCs with similar diameters (WT, 178.9 ± 7.3 μm, $n = 18$; AQP4 KO 166.3 ± 4.6 μm; $n = 23$; $p > .05$; unpaired Student's *t* test). Note that starting from D1 the AQP4 KO Mi was significantly reduced compared to WT. Data represents means ± SEM. A Two-way ANOVA and Bonferroni's Multiple Comparison Test were performed. ****$p < .0001$. Within each genotype, different letters on top of each bar indicate significant difference ($p < .05$) between them and equal letters indicate no significant difference ($n = 3$ independent experimental data set).

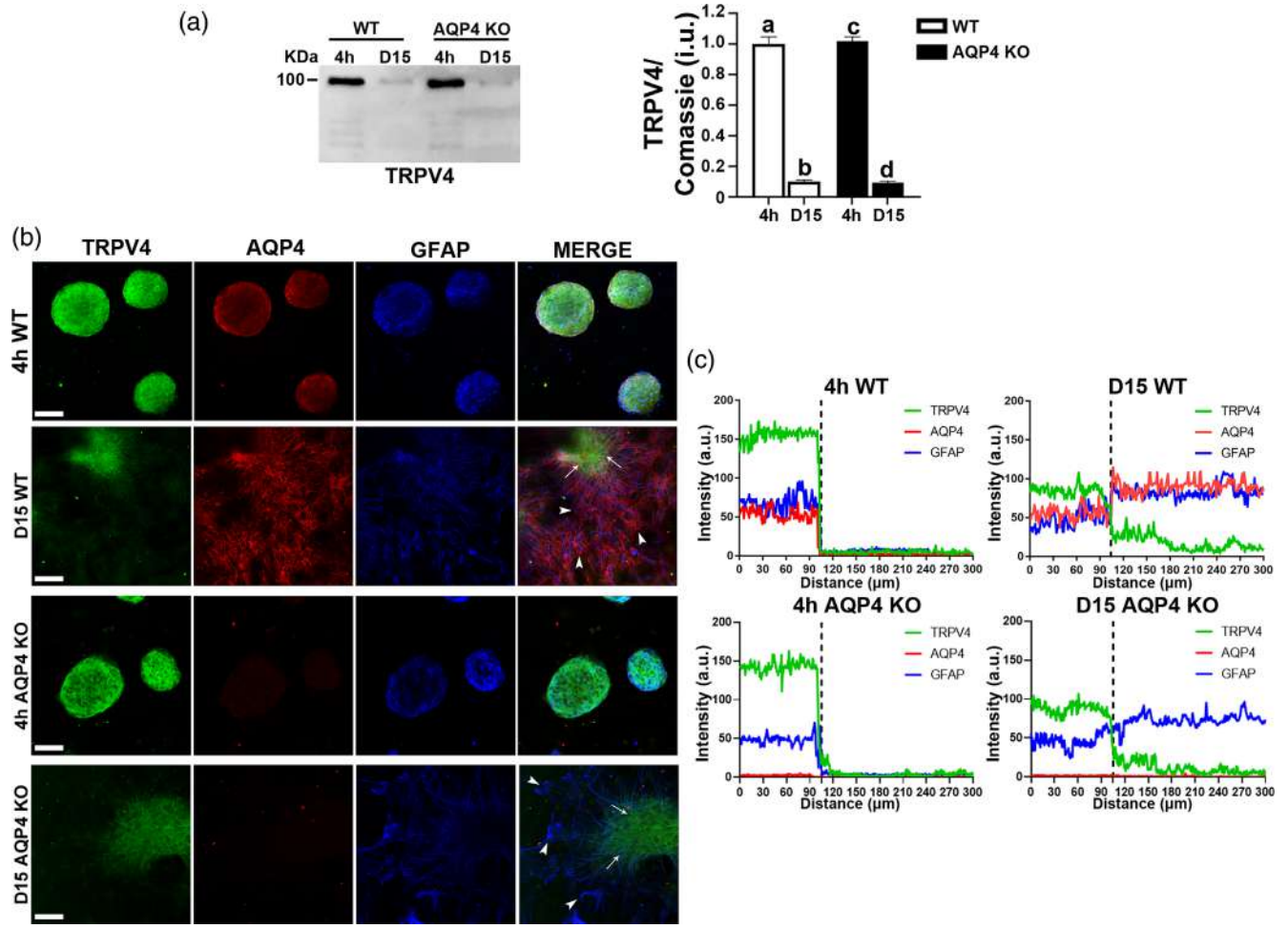

FIGURE 6 TRPV4 expression and distribution pattern in differentiated NSCs (a) Western blot analysis showing the time course of TRPV4 expression in WT and AQP4 KO (KO) NSCs undifferentiated (4 h) and differentiated for 15 days (D15). Note the decrease in TRPV4 expression during NSC differentiation. Coomassie blue-stained PVDF membrane was used as a loading control. Data represents means of intensity unit (i.u.) ± SEM. A Two-way ANOVA and Bonferroni's Multiple Comparison Test were performed. Within each genotype, different letters on top of each bar indicate significant differences ($p < .05$) between them ($n = 4$ independent experimental data). The molecular mass of marker (in kDa) is shown on the left of the gel. (b) Single-slice confocal images of TRPV4 (green), AQP4 (red), and GFAP (blue) expression and their merging in undifferentiated (4 h) and differentiated (D15) WT and AQP4 KO NSCs. TRPV4 was mostly expressed by cells located within the neurospheres (arrows). On the contrary, AQP4 and GFAP expression were detectable only in a few cells in undifferentiated neurospheres, but they were strongly expressed in cells migrating out of the sphere (arrowheads). Scale bar 100 μm. (c) Representative line scans showing TRPV4, AQP4, and GFAP fluorescence intensity in arbitrary units (a.u.) in undifferentiated (4 h) and differentiated (D15) WT and AQP4 KO NSCs from the center of the neurosphere cores (0 μm) to the outgrowth areas (up to 300 μm from the center of the core). Black dashed lines indicate the edges of neurosphere cores ($n = 14$ for WT and $n = 16$ for AQP4 KO neurospheres).

James, 2009; Stubbs et al., 2009). In this temporal frame, homeostatic mechanisms, such as buffering of extracellular K^+ and reduction of extracellular volume, develop with the help of glial cells (Connors et al., 1982).

4.1 | AQP4 and TRPV4 inversely correlated expression patterns in early postnatal stages

As already demonstrated for the rat cerebellum (Wen et al., 1999), we here found that the glial water channel AQP4 expression levels gradually increase during early postnatal development of both the brain and retina of WT mice and rats as well as in the in vitro cultured differentiating NSCs. However, we surprisingly observed an inversely correlated AQP4 trend for the TRPV4 channel, which was found to be downregulated in parallel.

By using the neurosphere model of astrocyte differentiation we here show that the AQP4 and TRPV4 opposite expression pattern with progressive AQP4 increase and TRPV4 decrease seems to be associated with astrocyte differentiation. Astrocyte differentiation occurs predominantly after birth between P10 and P16 in vivo (Catalani et al., 2002; Roessmann & Gambetti, 1986) while Müller cell differentiation is slightly delayed, occurring mainly during the second postnatal week (Weidman & Kuwabara, 1968). Interestingly, AQP4

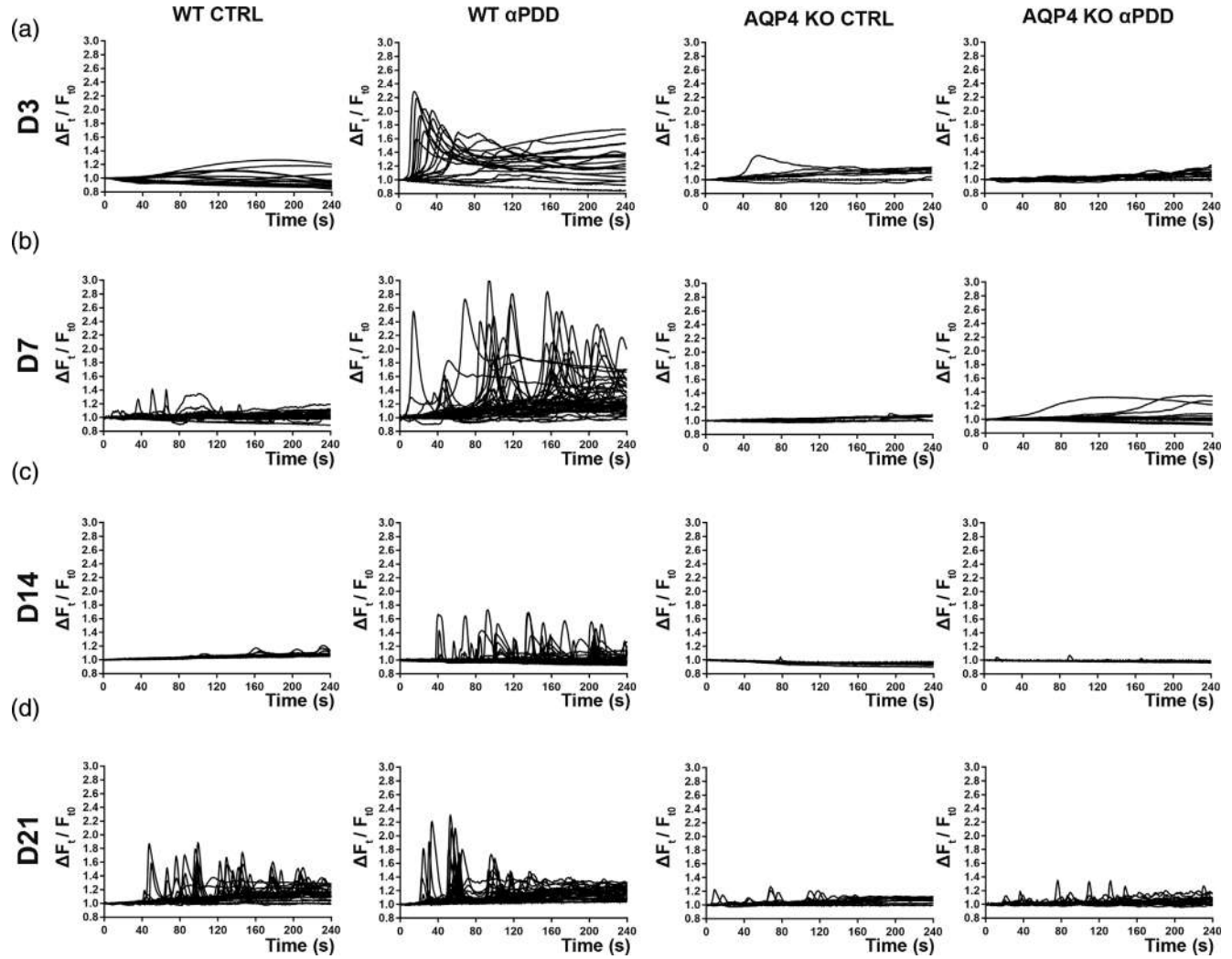

FIGURE 7 Basal and TRPV4-mediated-$[Ca^{2+}]$i dynamics in NSC from WT and AQP4 KO changes over time. Representative traces of fluorescence variation over time depicting $[Ca^{2+}]$i levels measured from WT and AQP4 KO NSCs in basal condition (CTRL) and after the exposure of the cells to 3 μM 4αPDD. Data were collected after 3 (D3, a), 7 (D7, b), 14 (D14, c), and 21 (D21, d) days in vitro.

protein expression in the retina is delayed by 1 week compared with the brain and starts to become detectable only during the second postnatal week. Of note, the observed AQP4 expression in the retina timely overlaps with (a) the deep vascular plexus and the mature vascular pattern formation (physiologically occurring at P14 and P21, respectively; Dorrell et al., 2002; Provis et al., 1997), (b) the regulation of extracellular fluid and K^+ spatial buffering operated by Müller cells (Nagelhus et al., 1998; Newman, 1987; Newman & Reichenbach, 1996), and (c) the change in water and ion composition of the extracellular space consequent to the opening of rodent eyelids (observed at P13–15) and the resulting light-induced neuronal activity (Seabrook et al., 2017). Based on these concomitant events, the increasingly augmented AQP4 expression levels could serve to modulate the responses of glial cells to the osmotic challenges deriving from neuronal transmission in maturing synapses. Moreover, it might drive or sustain those modeling processes occurring in the developing brain through the action of biomechanical forces exerted by AQP4-mediated water flows, as hypothesized (Papadopoulos & Verkman, 2013). In this regard, it is not surprising that the growth of the postnatal retina is driven by mechanical stimuli, such as the stretch of the developing sclera and the intraocular pressure (Mastronarde et al., 1984).

The biomechanical forces exerted by AQP4-mediated water flows in the developing brain and retina are useful to sustain major tissue remodeling, indicating possible parallel involvement of the Ca^{2+}-permeable mechanosensitive TRPV4 channel which is parallelly downregulated at later time points. Ca^{2+}-dependent processes such as cytoskeletal rearrangement, exocytosis, and gene expression are known to occur in the very early stages of postnatal life (Moody & Bosma, 2005). Therefore, one possible mechanism explaining the increasingly reduced expression of TRPV4 in the late postnatal phases (P14–4 M) is that it primarily takes part in the machinery that regulates the dynamic transition between immature and mature cellular patterns but is not so extensively required in the mature brain.

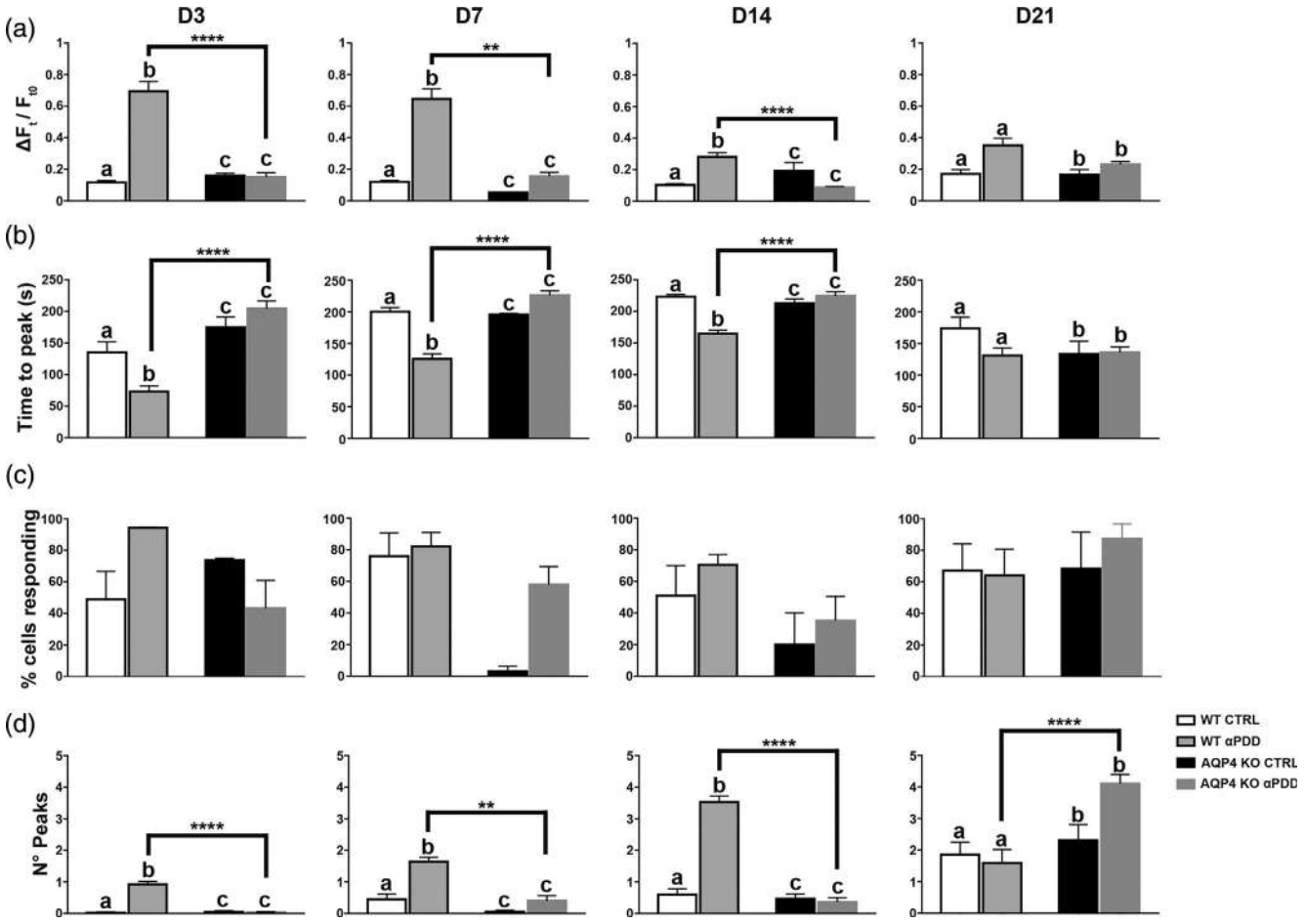

FIGURE 8 Quantitative analysis of $[Ca^{2+}]i$ fluorescence variation over time in Fluo-4-loaded WT and AQP4 KO NSC. Bar graphs showing (a) the averaged maximal $\Delta F_t/F_{t0}$, (b) the time to peak, (c) the percentage of responding cells and (d) the number of peaks of NSCs from WT and AQP4 KO in basal conditions (CTRL) and after the exposure of the cells to 3 μM 4αPDD at 3 (D3), 7 (D7), 14 (D14), and 21 (D21) days of culture. Data represent means ± SEM. The numbers of responding cells analyzed are reported in Table S1. A Two-way ANOVA and Bonferroni's Multiple Comparison Test were performed $^{**}p < .01$, and $^{****}p < .0001$. Within each genotype, different letters on top of each bar indicate significant differences ($p < .05$) between them and equal letters indicate no significant differences.

4.2 | AQP4-dependent TRPV4 glial expression

In our study, we have demonstrated that the deletion of AQP4 is associated with downregulation of TRPV4 protein levels specifically in the developing retina, while no significant differences were detected in the brain and NSCs, indicating AQP4 dependent-TRPV4 downregulation to be specifically ascribed to Müller cells and not to astrocytes, and that distinct mechanisms of functional interaction between TRPV4 and AQP4 occur in astrocytes and Müller cells. Previous studies on adult AQP4 KO mouse retinas have shown a mild decrease in TRPV4 mRNA levels, with no observed differences in terms of layering, cytoarchitecture, and Müller glial morphology (Jo et al., 2015). This discrepancy may arise from the different approaches employed in the two studies. Our study utilized Western blot analysis to directly assess protein levels, while Jo et al. used qPCR, which measures mRNA expression. Differences between mRNA and protein expression levels may be ascribed to post-transcriptional regulatory mechanisms that influence the translation and stability of mRNA into functional proteins as well as post-translational stability of TRPV4 protein in the cell plasma membrane of retinal cells due to the absence of a potential functional partner such as AQP4. Furthermore, the unaltered TRPV4 immunoreactivity observed in their study might be attributed to their focus on TRPV4 localization alone, while ours, comprehensively assessed both the localization and extent of differential expression throughout the entire retinal thickness, revealing differences in deeper layers.

The mice here used are AQP4 KO CD1 mice, generated through targeted gene disruption (Basco et al., 2013; Fan et al., 2005), and characterized by a mild phenotype. However, different AQP4 KO mice have been reported, generated with both constitutive deficiency in AQP4 (Fan et al., 2005; Ikeshima-Kataoka et al., 2013; Ma et al., 1997), as well as mice with glial-conditional AQP4 deficiency (Haj-Yasein et al., 2011).

These mouse models displayed normal phenotypic characteristics in terms of growth, development, survival, and neuromuscular function (Ma et al., 1997; Manley et al., 2000; Ozawa et al., 2019), with

only a mild impairment related to urinary concentration (Fan et al., 2005; Ma et al., 1997). In the CNS, they exhibited regular brain structure, vascular anatomy, baseline intracranial pressure (ICP), intracranial compliance, and blood–brain barrier function (Fan et al., 2005; Saadoun et al., 2009; Yao et al., 2008; Zeng et al., 2007). However, they also showed deficiencies in both cognition and memory (Fan et al., 2005; Ma et al., 1997; Skucas et al., 2011; Zhang et al., 2013), an increase in extracellular space (Yao et al., 2008), elevated K^+ concentration (Strohschein et al., 2011), reduced glutamate uptake (Zeng et al., 2007) and brain water uptake after systemic hypoosmotic stress (Haj-Yasein et al., 2011). Therefore, if AQP4 KO mice have been largely used as a valuable model to study various aspects of brain physiology and neurological disorders, as any other study performed using genetically modified animals, we cannot completely exclude some molecular changes observed as secondary effects to the knockout strategy.

We here also reported that the selective ablation of the AQP4 channel does not affect the expression of the Muller cell marker GS during retinal postnatal development. This result was not unexpected, as in a previous paper (Nicchia et al., 2016), we demonstrated by western blotting and immunofluorescence that there was no difference in the expression and distribution of GS at the protein level in the adult retina (5–10 months old) of AQP4 KO mice compared to WT. However, these findings appear to contrast with those published by Ozawa et al. (2019), reporting a reduction in GS expression at mRNA level in AQP4 KO retina using qPCR. This discrepancy may arise from the different analysis of GS protein (Nicchia et al., 2016) versus GS mRNA (Ozawa et al., 2019) and/or from the use of different AQP4 KO mouse models with different genetic backgrounds. It is worth noting that a study by Li et al. (Li et al., 2014), performed on the same AQP4 KO mouse model used in the present study shows that deletion of AQP4 did not affect the basic levels of GS expression in the retina.

Complementing evidence obtained in the NSC in vitro model for early cortex gliogenesis showed a similar trend for AQP4 and TRPV4 postnatal expression patterns. This model allowed us to focus on the astrocyte differentiation process which is a central event in brain and retina development (Freeman, 2010; Scemes et al., 2003; Sloan & Barres, 2014; Sofroniew & Vinters, 2010; Von Visger et al., 1994). As observed in in vivo astrocytes and Müller cells, TRPV4 expression decreases during NSCs in vitro differentiation into astrocytes. When TRPV4 is strongly expressed in undifferentiated floating neurospheres its expression appears to be confined to the core during NSC differentiation into astrocytes. These results indicate that TRPV4 is likely to play a major role in neural progenitors and precursor cells rather than in differentiated cells.

On the other hand, AQP4 was initially detected in a few cells at the periphery of neurospheres, whereas at later time points, it was found in GFAP-positive cells of the spreading outgrowth. In line with results obtained in the brain and retina, this data suggests that AQP4 is required for later stages of gliogenesis and, probably, for cell migration occurring during NSC differentiation, as demonstrated in other cell types (Auguste et al., 2006; Saadoun et al., 2005).

4.3 | AQP4 different aggregation states into astrocyte differentiation and migration

By providing an accurate tool for the study of gliogenesis, NSCs further enabled us to investigate the molecular and functional properties of AQP4-OAP supramolecular aggregates and their role in astrocyte differentiation and migration. The biochemical separation of different-sized AQP4 aggregates performed in differentiating neurospheres and in developing retina showed that the progressively increasing expression of AQP4 occurred in parallel with AQP4 supramolecular structures of progressively growing size. If this is in line with the role of OAPs in astrocyte differentiation proposed by Smith et al. (Smith et al., 2014), these data also seem to indicate that the aggregation state of AQP4 is strictly linked to the abundance of AQP4 expression in the plasma membrane: the greater the AQP4 amount is, the larger is the size of AQP4 assemblies. The increase in AQP4 expression could therefore address the need to have large AQP4 assemblies in turn promoting astrocyte differentiation. As indirect evidence in support of this, we previously demonstrated that AQP4 impairment in forming OAPs in the OAP null mice (de Bellis et al., 2021) resulted in a significant reduction in AQP4 total expression level, indicating a strict interdependence between AQP4 total expression levels and OAP formation and size.

As the differentiating astrocytes are characterized by a progressive increase in AQP4 expression temporally associated with AQP4 aggregation into OAPs, we next addressed a key question related to the role of AQP4 in cell migration. Leading-edge polarization of AQP4 was reported in migrating cells in culture (Papadopoulos et al., 2008; Saadoun et al., 2005). Although the specific molecular mechanisms remain unclear, a proposed hypothesis suggests that AQP4-mediated water influx at the leading edge leads to localized cell swelling therefore favoring cell membrane protrusion and migration (Papadopoulos et al., 2008). Glial progenitors move along radial glial fibers to reach the pial surface of the brain (Barry et al., 2014). Astrocytes can also undergo tangential migration, a crucial process for the dispersion of astrocytes to different regions of the CNS (Kazanis et al., 2008). Astrocyte migration continues throughout early brain development and even into adulthood (Felix et al., 2021). The increase in plasma water transport rate we found in differentiating neurospheres could be related to the known role of AQP4 in sustaining astrocyte migration as well as their proper spatial distribution and functional integration within the CNS.

Further studies have also revealed that the water influx at the leading edge of the cell would be mediated by AQP4 tetramers and small OAPs. In contrast, large OAPs exhibit limited mobility in the plasma membrane and are involved in facilitating cell adhesion and polarization rather than migration (Smith et al., 2014). Therefore, to investigate whether AQP4 and its aggregation state could influence the migration of differentiating glial progenitors, we measured the migratory index of neurospheres in the absence of AQP4 and during differentiation into astrocytes. Consistent with previous reports (Kong et al., 2008), we observed that migration is greatly impaired in the absence of AQP4. New information came from the analysis of

differentiating neurospheres that, although characterized by a progressive increase in OAP level and size, displayed a progressive increase in the migratory index, in apparent contrast with the role of OAPs in astrocyte adhesion and not in astrocyte migration as postulated by Smith et al. (2014). One possible explanation is that the biomechanical forces generated by AQP4-mediated water flows prevail over the finest changes associated with the different states of aggregation. We can speculate that tetramers and smaller AQP4 assemblies would improve the cell migration of the earliest glial cell precursors to reach the brain layer target into the developing brain, contributing to the formation of functional neural circuits. In parallel, the progressive increase in AQP4 expression level and the progressive formation of large-size OAPs would promote AQP4 polarization at the glial endfoot maximizing the water permeability (Nico et al., 2001).

4.4 | TRPV4 and calcium

Previous studies indicated that the profile of the temporal dynamics of the response to TRPV4 agonist observed in primary Dorsal Root Ganglion neurons (Alexander et al., 2013), in astrocytes (Benfenati et al., 2007) or mesenchymal stem cells (Gilchrist et al., 2019) could be variable and it can be divided into two main types: some cells exhibited a transient oscillatory increase in calcium with a short time to peak and a lower duration which then returned to baseline, whereas others showed a prolonged elevation in calcium over time, which was defined as a sustained response (Alexander et al., 2013). The analysis of the temporal dynamics of the calcium response to 4αPDD in WT NSCs, during differentiation from D3 to D21, revealed an oscillatory behavior, with a short time to peak and elevated peak number, indicating that the distinct balance between a decreasing TRPV4 and an increasing AQP4 expression determines different combinations of responses to the 4αPDD agonist. These differences are even more pronounced between WT and AQP4 KO NSCs with AQP4 ablation causing a massive reduction in calcium responses to the 4αPDD agonist AQP4 KO NSCs predominantly exhibit, when present, dynamics typical of a sustained response with a longer time to peak and a lower number of peaks. The mechanism beyond different responses to the agonist has not been clarified. However, studies reported that agonists could promote the translocation of TRPV4 protein pools in the plasma membrane (Baratchi et al., 2019), which might affect the magnitude and the dynamics of the response. Thus, it is plausible that the absence of AQP4 may cause altered sensitivity to the agonist and/or promote the internalization of that might explain the difference observed in calcium dynamics.

The different temporal patterns of calcium transients resulting from AQP4 and TRPV4 coordinated activity might differentially regulate cell processes, such as cellular migration and proliferation. In this regard, AQP4 may promote calcium influx through TRPV4, which directly mediates actin depolymerization (Disanza et al., 2005; Yoneda et al., 2000). Finely tuned spatiotemporal water and calcium dynamics are consistent with the central role played by astrocytes in monitoring and dynamically responding to changes occurring during early postnatal development.

5 | CONCLUSIONS

We observed a distinct temporal expression pattern for AQP4 and TRPV4 in the brain compared to the retina probably due to different mechanisms of TRPV4 and AQP4 functional interaction in astrocytes and Müller cells during development. We provided evidence that during differentiation a finely tuned AQP4 and TRPV4 expression is orchestrated by astrocytes with a progressive TRPV4 decrease and AQP4 increase this latter is also characterized by a plasma membrane organization into larger-sized assemblies (OAPs). As a result, astrocytes progressively acquire increased plasma membrane water permeability and cell migration and undergo strong variation in terms of Ca^{2+} signaling. These functional changes might play a key role in sustaining the biochemical and physiological mechanisms responsible for astrocyte differentiation during brain and retinal development.

AUTHOR CONTRIBUTIONS

A.C., M.G.M., and G.P.N.: conceptualization, validation, and investigation. A.C., M.G.M., E.S., B.B., P.A., G.M., A.R., D.S., G.P.N.: methodology and formal analysis. A.C., M.G.M., B.B., E.S. and G.M.: data curation. A.C., M.G.M. and G.P.N.: writing—original draft preparation. A.C., M.G.M., B.B., D.C.S., E.S., A.F., V.B., and G.P.N.: writing—review and editing. G.P.N.: supervision and project administration. G.P.N., A.F., and V.B.: funding acquisition.

ACKNOWLEDGMENTS

AstroDyn (FA9550-19-1-0370) and AstroColl (FA9550-21-1-00352) funded by AFOSR to GPN and VB; Stochastic Biophysical Interactions within Aquaporin-4 Assemblies (FA9550-20-1-0324) and The Stochastic Biophysics Controlling AQP4 Regulation and Self-Assembly (FA9550-23-1-0583) funded by AFOSR to GPN; AstroLight (FA9550-20-1-0386) and AstroTalk (FA9550-23-1-0736) funded by AFOSR to VB, ES and DS. ASTROTECH (GA956325), Marie Skłodowska-Curie Actions-ITN-2020 funded by the European Commission to GPN and VB. We acknowledge the following co-fundings from Next Generation EU, in the context of the National Recovery and Resilience Plan: project CN00000041 – National Center for Gene Therapy and Drugs based on RNA Technology (DD n.1035, 17.06.2022) to GPN and AF; investment PE12—project MNESYS: "A multiscale integrated approach to the study of the nervous system in healt and disease" (DD n.1553, 11.10.2022) to GPN and AF; investment PE8—project Age-It: "Ageing Well in an Ageing Society" (DM n.1557, 11.10.2022) to AF. The views and opinions expressed are those of the authors only and do not necessarily reflect those of the European Union or the European Commission. Neither the European Union nor the European Commission can be held responsible for them. HORIZON EUROPE SEEDS INTERGLIO (S08) funded by the University of Bari Aldo Moro to GPN and AF. PON Research and Innovation 2014–2020 DM1062/2021 (FSE-REACT EU, Action IV.6) cofounded by the University of

Bari Aldo Moro and the European Union to AC. POR Puglia 2014–2020-asse X-Action 10.4, Research for Innovation-REFIN to MGM. The authors would like to thank Gaetano Devito for his excellent technical assistance and Richard Lusardi for his expert assistance in revising the English.

DATA AVAILABILITY STATEMENT

The data described in the manuscript are contained within the manuscript.

ORCID

Antonio Cibelli https://orcid.org/0000-0001-5689-9885
Maria Grazia Mola https://orcid.org/0000-0002-4421-9237
Emanuela Saracino https://orcid.org/0000-0001-9140-3128
Barbara Barile https://orcid.org/0000-0002-5093-6662
Guido Mogni https://orcid.org/0000-0003-0423-5942
Eliana Scemes https://orcid.org/0000-0002-6650-3976
Antonio Frigeri https://orcid.org/0000-0002-5284-2934
Grazia Paola Nicchia https://orcid.org/0000-0002-4257-514X

REFERENCES

Alexander, R., Kerby, A., Aubdool, A. A., Power, A. R., Grover, S., Gentry, C., & Grant, A. D. (2013). 4α-phorbol 12,13-didecanoate activates cultured mouse dorsal root ganglia neurons independently of TRPV4. *British Journal of Pharmacology*, *168*, 761–772.

Auguste, K. I., Jin, S., Uchida, K., Yan, D., Manley, G. T., Papadopoulos, M. C., & Verkman, A. S. (2006). Greatly impaired migration of implanted aquaporin-4-deficient astroglial cells in mouse brain toward a site of injury. *The FASEB Journal*, *21*, 108–116. https://doi.org/10.1096/fj.06-6848com

Baratchi, S., Keov, P., Darby, W. G., Lai, A., Khoshmanesh, K., Thurgood, P., Vahidi, P., Ejendal, K., & McIntyre, P. (2019). The TRPV4 agonist GSK1016790A regulates the membrane expression of TRPV4 channels. *Frontiers in Pharmacology*, *10*, 6.

Barry, D. S., Pakan, J. M. P., & McDermott, K. W. (2014). Radial glial cells: Key organisers in CNS development. *The International Journal of Biochemistry & Cell Biology*, *46*, 76–79.

Basco, D., Blaauw, B., Pisani, F., Sparaneo, A., Nicchia, G. P., Mola, M. G., Reggiani, C., Svelto, M., & Frigeri, A. (2013). AQP4-dependent water transport plays a functional role in exercise-induced skeletal muscle adaptations. *PLoS One*, *8*, 23520529.

Bautch, V. L., & James, J. M. (2009). Neurovascular development: The beginning of a beautiful friendship. *Cell Adhesion & Migration*, *3*, 199–204.

Beattie, R., & Hippenmeyer, S. (2017). Mechanisms of radial glia progenitor cell lineage progression. *FEBS Letters*, *591*, 3993–4008.

Benfenati, V., Amiry-Moghaddam, M., Caprini, M., Mylonakou, M. N., Rapisarda, C., Ottersen, O. P., & Ferroni, S. (2007). Expression and functional characterization of transient receptor potential vanilloid-related channel 4 (TRPV4) in rat cortical astrocytes. *Neuroscience*, *148*, 876–892.

Benfenati, V., Caprini, M., Dovizio, M., Mylonakou, M. N., Ferroni, S., Ottersen, O. P., & Amiry-Moghaddam, M. (2011). An aquaporin-4/transient receptor potential vanilloid 4 (AQP4/TRPV4) complex is essential for cell-volume control in astrocytes. *Proceedings of the National Academy of Sciences of the United States of America*, *108*, 2563–2568.

Bentivoglio, M., & Mazzarello, P. (1999). The history of radial glia. *Brain Research Bulletin*, *49*, 305–315.

Bringmann, A., Pannicke, T., Grosche, J., Francke, M., Wiedemann, P., Skatchkov, S. N., Osborne, N. N., & Reichenbach, A. (2006). Müller cells in the healthy and diseased retina. *Progress in Retinal and Eye Research*, *25*, 397–424.

Catalani, A., Sabbatini, M., Consoli, C., Cinque, C., Tomassoni, D., Azmitia, E., Angelucci, L., & Amenta, F. (2002). Glial fibrillary acidic protein immunoreactive astrocytes in developing rat hippocampus. *Mechanisms of Ageing and Development*, *123*, 481–490.

Ciappelloni, S., Bouchet, D., Dubourdieu, N., Boué-Grabot, E., Kellermayer, B., Manso, C., Marignier, R., Oliet, S. H. R., Tourdias, T., & Groc, L. (2019). Aquaporin-4 surface trafficking regulates astrocytic process motility and synaptic activity in health and autoimmune disease. *Cell Reports*, *27*, 3860–3872.e4.

Connors, B., Gutnick, M., & Prince, D. (1982). Electrophysiological properties of neocortical neurons in vitro. *Journal of Neurophysiology*, *48*, 1302–1320.

Crane, J. M., Van Hoek, A. N., Skach, W. R., & Verkman, A. S. (2008). Aquaporin-4 dynamics in orthogonal arrays in live cells visualized by quantum dot single particle tracking. *Molecular Biology of the Cell*, *19*, 3369–3378.

de Bellis, M., Cibelli, A., Mola, M. G., Pisani, F., Barile, B., Mastrodonato, M., Banitalebi, S., Amiry-Moghaddam, M., Abbrescia, P., Frigeri, A., Svelto, M., & Nicchia, G. P. (2021). Orthogonal arrays of particle assembly are essential for normal aquaporin-4 expression level in the brain. *Glia*, *69*, 473–488.

Diana, A., Setzu, M. D., Kokaia, Z., Nat, R., Maxia, C., & Murtas, D. (2021). SmartFlareTM is a reliable method for assessing mRNA expression in single neural stem cells. *World Journal of Stem Cells*, *13*, 1918–1927.

Disanza, A., Steffen, A., Hertzog, M., Frittoli, E., Rottner, K., & Scita, G. (2005). Actin polymerization machinery: The finish line of signaling networks, the starting point of cellular movement. *Cellular and Molecular Life Sciences*, *62*, 955–970.

Dorrell, M. I., Aguilar, E., & Friedlander, M. (2002). Retinal vascular development is mediated by endothelial filopodia, a preexisting astrocytic template and specific R-cadherin adhesion. *Investigative Ophthalmology & Visual Science*, *43*, 3500–3510.

Duval, N., Gomès, D., Calaora, V., Calabrese, A., Meda, P., & Bruzzone, R. (2002). Cell coupling and Cx43 expression in embryonic mouse neural progenitor cells. *Journal of Cell Science*, *115*, 3241–3251.

Fan, Y., Zhang, J., Sun, X. L., Gao, L., Zeng, X. N., Ding, J. H., Cao, C., Niu, L., & Hu, G. (2005). Sex- and region-specific alterations of basal amino acid and monoamine metabolism in the brain of aquaporin-4 knockout mice. *Journal of Neuroscience Research*, *82*, 458–464.

Felix, L., Stephan, J., & Rose, C. R. (2021). Astrocytes of the early postnatal brain. *European Journal of Neuroscience*, *54*, 5649–5672.

Freeman, M. R. (2010). Specification and morphogenesis of astrocytes. *Science*, *330*, 774–778. https://doi.org/10.1126/science.1190928

Furman, C. S., Gorelick-Feldman, D. A., Davidson, K. G. V., Yasumura, T., Neely, J. D., Agre, P., & Rash, J. E. (2003). Aquaporin-4 square array assembly: Opposing actions of M1 and M23 isoforms. *Proceedings of the National Academy of Sciences of the United States of America*, *100*, 13609–13614.

Gardner-Medwin, A. R. (1983). A study of the mechanisms by which potassium moves through brain tissue in the rat. *The Journal of Physiology*, *335*, 353–374.

Gilchrist, C. L., Leddy, H. A., Kaye, L., Case, N. D., Rothenberg, K. E., Little, D., Liedtke, W., Hoffman, B. D., & Guilak, F. (2019). TRPV4-mediated calcium signaling in mesenchymal stem cells regulates aligned collagen matrix formation and vinculin tension. *Proceedings of the National Academy of Sciences of the United States of America*, *116*, 1992–1997.

Gonmanee, T., Arayapisit, T., Vongsavan, K., Phruksaniyom, C., & Sritanaudomchai, H. (2021). Optimal culture conditions for neurosphere formation and neuronal differentiation from human dental pulp stem cells. *Journal of Applied Oral Science*, *29*, e20210296.

Haj-Yasein, N. N., Vindedal, G. F., Eilert-Olsen, M., Gundersen, G. A., Skare, Ø., Laake, P., Klungland, A., Thorén, A. E., Burkhardt, J. M., Ottersen, O. P., & Nagelhus, E. A. (2011). Glial-conditional deletion of aquaporin-4 (Aqp4) reduces blood-brain water uptake and confers barrier function on perivascular astrocyte endfeet. *Proceedings of the National Academy of Sciences of the United States of America*, *108*, 17815–17820.

Heo, J., Meng, F., & Hua, S. Z. (2008). Contribution of aquaporins to cellular water transport observed by a microfluidic cell volume sensor. *Analytical Chemistry*, *80*, 6974–6980.

Hiroaki, Y., Tani, K., Kamegawa, A., Gyobu, N., Nishikawa, K., Suzuki, H., Walz, T., Sasaki, S., Mitsuoka, K., Kimura, K., Mizoguchi, A., & Fujiyoshi, Y. (2006). Implications of the aquaporin-4 structure on array formation and cell adhesion. *Journal of Molecular Biology*, *355*, 628–639.

Ikeshima-Kataoka, H., Abe, Y., Abe, T., & Yasui, M. (2013). Immunological function of aquaporin-4 in stab-wounded mouse brain in concert with a pro-inflammatory cytokine inducer, osteopontin. *Molecular and Cellular Neurosciences*, *56*, 65–75.

Jo, A. O., Ryskamp, D. A., Phuong, T. T. T., Verkman, A. S., Yarishkin, O., MacAulay, N., & Križaj, D. (2015). TRPV4 and AQP4 channels synergistically regulate cell volume and calcium homeostasis in retinal Muller glia. *Journal of Neuroscience*, *35*, 13525–13537. https://doi.org/10.1523/JNEUROSCI.1987-15.2015

Kazanis, I., Lathia, J., Moss, L., & ffrench-Constant, C. (2008). The neural stem cell microenvironment. In *Stembook*. Harvard Stem Cell Institute.

Kong, H., Fan, Y., Xie, J., Ding, J., Sha, L., Shi, X., Sun, X., & Hu, G. (2008). AQP4 knockout impairs proliferation, migration and neuronal differentiation of adult neural stem cells. *Journal of Cell Science*, *121*, 4029–4036.

Küppers, E., Gleiser, C., Brito, V., Wachter, B., Pauly, T., Hirt, B., & Grissmer, S. (2008). AQP4 expression in striatal primary cultures is regulated by dopamine – Implications for proliferation of astrocytes. *European Journal of Neuroscience*, *28*, 2173–2182. https://doi.org/10.1111/j.1460-9568.2008.06531.x

Lafrenaye, A. D., & Simard, J. M. (2019). Bursting at the seams: Molecular mechanisms mediating astrocyte swelling. *International Journal of Molecular Sciences*, *20*, 30650535.

Lehmenkühler, A., Syková, E., Svoboda, J., Zilles, K., & Nicholson, C. (1993). Extracellular space parameters in the rat neocortex and subcortical white matter during postnatal development determined by diffusion analysis. *Neuroscience*, *55*, 339–351.

Li, X. M., Le, W. R., Yao, J., Ren, Y., Zhao, Y. X., Cao, G. F., Qin, J., & Yan, B. (2014). Abnormal glutamate metabolism in the retina of aquaporin 4 (AQP4) knockout mice upon light damage. *Neurological Sciences*, *35*, 847–853.

Liu, X., Bandyopadhyay, B., Nakamoto, T., Singh, B., Liedtke, W., Melvin, J. E., & Ambudkar, I. (2006). A role for AQP5 in activation of TRPV4 by hypotonicity: Concerted involvement of AQP5 and TRPV4 in regulation of cell volume recovery. *The Journal of Biological Chemistry*, *281*, 15485–15495.

Ma, T., Yang, B., Gillespie, A., Carlson, E. J., Epstein, C. J., & Verkman, A. S. (1997). Generation and phenotype of a transgenic knockout mouse lacking the mercurial-insensitive water channel aquaporin-4. *Journal of Clinical Investigation*, *100*, 957–962.

Manley, G. T., Fujimura, M., Ma, T., Noshita, N., Filiz, F., Bollen, A. W., Chan, P., & Verkman, A. S. (2000). Aquaporin-4 deletion in mice reduces brain edema after acute water intoxication and ischemic stroke. *Nature Medicine*, *6*, 159–163.

Mastronarde, D. N., Thibeault, M. A., & Dubin, M. W. (1984). Non-uniform postnatal growth of the cat retina. *Journal of Comparative Neurology*, *228*, 598–608.

Mola, M. G., Nicchia, G. P., Svelto, M., Spray, D. C., & Frigeri, A. (2009). Automated cell-based assay for screening of aquaporin inhibitors. *Analytical Chemistry*, *81*, 8219–8229.

Mola, M. G., Saracino, E., Formaggio, F., Amerotti, A. G., Barile, B., Posati, T., Cibelli, A., Frigeri, A., Palazzo, C., Zamboni, R., Caprini, M., Nicchia, G. P., & Benfenati, V. (2021). Cell volume regulation mechanisms in differentiated astrocytes. *Cellular Physiology and Biochemistry*, *55*, 196–212.

Mola, M. G., Sparaneo, A., Gargano, C. D., Spray, D. C., Svelto, M., Frigeri, A., Scemes, E., & Nicchia, G. P. (2016). The speed of swelling kinetics modulates cell volume regulation and calcium signaling in astrocytes: A different point of view on the role of aquaporins. *Glia*, *64*, 139–154.

Moody, W. J., & Bosma, M. M. (2005). Ion channel development, spontaneous activity, and activity-dependent development in nerve and muscle cells. *Physiological Reviews*, *85*, 883–941.

Nagelhus, E. A., Veruki, M. L., Torp, R., Haug, F. M., Laake, J. H., Nielsen, S., Agre, P., & Ottersen, O. P. (1998). Aquaporin-4 water channel protein in the rat retina and optic nerve: Polarized expression in Müller cells and fibrous astrocytes. *The Journal of Neuroscience*, *18*, 2506–2519.

Neely, J. D., Christensen, B. M., Nielsen, S., & Agre, P. (1999). Heterotetrameric composition of aquaporin-4 water channels. *Biochemistry*, *38*, 11156–11163.

Newman, E., & Reichenbach, A. (1996). The Muller cell: A functional element of the retina. *Trends in Neurosciences*, *19*, 307–312.

Newman, E. A. (1987). Distribution of potassium conductance in mammalian Müller (glial) cells: A comparative study. *The Journal of Neuroscience*, *7*, 2423–2432.

Nicchia, G. P., Pisani, F., Simone, L., Cibelli, A., Mola, M. G., Dal Monte, M., Frigeri, A., Bagnoli, P., & Svelto, M. (2016). Glio-vascular modifications caused by Aquaporin-4 deletion in the mouse retina. *Experimental Eye Research*, *146*, 259–268.

Nicchia, G. P., Rossi, A., Nudel, U., Svelto, M., & Frigeri, A. (2008). Dystrophin-dependent and -independent AQP4 pools are expressed in the mouse brain. *Glia*, *56*, 869–876.

Nicholson, C., & Hrabětová, S. (2017). Brain extracellular space: The final frontier of neuroscience. *Biophysical Journal*, *113*, 2133–2142.

Nico, B., Frigeri, A., Nicchia, G. P., Quondamatteo, F., Herken, R., Errede, M., Ribatti, D., Svelto, M., & Roncali, L. (2001). Role of aquaporin-4 water channel in the development and integrity of the blood-brain barrier. *Journal of Cell Science*, *114*, 1297–1307.

Ozawa, Y., Toda, E., Kawashima, H., Homma, K., Osada, H., Nagai, N., Abe, Y., Yasui, M., & Tsubota, K. (2019). Aquaporin 4 suppresses neural hyperactivity and synaptic fatigue and fine-tunes neurotransmission to regulate visual function in the mouse retina. *Molecular Neurobiology*, *56*, 8124–8135.

Panchision, D. M., Chen, H.-L., Pistollato, F., Papini, D., Ni, H.-T., & Hawley, T. S. (2007). Optimized flow cytometric analysis of central nervous system tissue reveals novel functional relationships among cells expressing CD133, CD15, and CD24. *Stem Cells*, *25*, 1560–1570.

Papadopoulos, M. C., Saadoun, S., & Verkman, A. S. (2008). Aquaporins and cell migration. *Pflügers Archiv*, *456*, 693–700.

Papadopoulos, M. C., & Verkman, A. S. (2013). Aquaporin water channels in the nervous system. *Nature Reviews. Neuroscience*, *14*, 265–277.

Provis, J. M., Leech, J., Diaz, C. M., Penfold, P. L., Stone, J., & Keshet, E. (1997). Development of the human retinal vasculature: Cellular relations and VEGF expression. *Experimental Eye Research*, *65*, 555–568.

Rakic, P. (2003). Developmental and evolutionary adaptations of cortical radial glia. *Cerebral Cortex*, *13*, 541–549.

Rash, J. E., Davidson, K. G. V., Yasumura, T., & Furman, C. S. (2004). Freeze-fracture and immunogold analysis of aquaporin-4 (AQP4) square arrays, with models of AQP4 lattice assembly. *Neuroscience*, *129*, 915–934.

Raymond, P. A., Barthel, L. K., Bernardos, R. L., & Perkowski, J. J. (2006). Molecular characterization of retinal stem cells and their niches in adult zebrafish. *BMC Developmental Biology*, *6*, 16872490.

Reynolds, B. A., & Weiss, S. (1996). Clonal and population analyses demonstrate that an EGF-responsive mammalian embryonic CNS precursor is a stem cell. *Developmental Biology*, *175*, 1–13.

Rice, D., & Barone, S. (2000). Critical periods of vulnerability for the developing nervous system: Evidence from humans and animal models. *Environmental Health Perspectives*, *108*(Suppl 3), 511–533.

Ritzmann, D., Jahn, M., Heck, S., Jung, C., Cesetti, T., Couturier, N., Rudolf, R., Reuscher, N., Buerger, C., Rauh, O., & Fauth, T. (2023). The Ca2+ channel TRPV4 is dispensable for Ca2+ influx and cell volume regulation during hypotonic stress response in human keratinocyte cell lines. *Cell Calcium*, *111*, 102715.

Roessmann, U., & Gambetti, P. (1986). Astrocytes in the developing human brain. *Acta Neuropathologica*, *70*, 308–313. https://doi.org/10.1007/BF00686089

Ryskamp, D. A., Witkovsky, P., Barabas, P., Huang, W., Koehler, C., Akimov, N. P., Lee, S. H., Chauhan, S., Xing, W., Renteria, R. C., Liedtke, W., & Krizaj, D. (2011). The polymodal ion channel transient receptor potential vanilloid 4 modulates calcium flux, spiking rate, and apoptosis of mouse retinal ganglion cells. *Journal of Neuroscience*, *31*, 7089–7101. https://doi.org/10.1523/JNEUROSCI.0359-11.2011

Saadoun, S., Papadopoulos, M. C., Watanabe, H., Yan, D., Manley, G. T., & Verkman, A. S. (2005). Involvement of aquaporin-4 in astroglial cell migration and glial scar formation. *Journal of Cell Science*, *118*, 5691–5698.

Saadoun, S., Tait, M. J., Reza, A., Davies, D. C., Bell, B. A., Verkman, A. S., & Papadopoulos, M. C. (2009). AQP4 gene deletion in mice does not alter blood-brain barrier integrity or brain morphology. *Neuroscience*, *161*, 764–772.

Salman, M. M., Kitchen, P., Woodroofe, M. N., Brown, J. E., Bill, R. M., Conner, A. C., & Conner, M. T. (2017). Hypothermia increases aquaporin 4 (AQP4) plasma membrane abundance in human primary cortical astrocytes via a calcium/transient receptor potential vanilloid 4 (TRPV4)- and calmodulin-mediated mechanism. *The European Journal of Neuroscience*, *46*, 2542–2547.

Saunders, N. R., Liddelow, S. A., & Dziegielewska, K. M. (2012). Barrier mechanisms in the developing brain. *Frontiers in Pharmacology*, *3*, 46.

Scemes, E., Duval, N., & Meda, P. (2003). Reduced expression of P2Y1 receptors in connexin43-null mice alters calcium signaling and migration of neural progenitor cells. *The Journal of Neuroscience*, *23*, 11444–11452.

Schaägger, H., Cramer, W. A., & von Jagow, G. (1994). Analysis of molecular masses and oligomeric states of protein complexes by blue native electrophoresis and isolation of membrane protein complexes by two-dimensional native electrophoresis. *Analytical Biochemistry*, *217*, 220–230.

Seabrook, T. A., Burbridge, T. J., Crair, M. C., & Huberman, A. D. (2017). Architecture, function, and assembly of the mouse visual system, *40*, 499–538. https://doi.org/10.1146/annurev-neuro-071714-033842

Semple, B. D., Blomgren, K., Gimlin, K., Ferriero, D. M., & Noble-Haeusslein, L. J. (2013). Brain development in rodents and humans: Identifying benchmarks of maturation and vulnerability to injury across species. *Progress in Neurobiology*, *106-107*, 1–16.

Silberstein, C., Bouley, R., Huang, V., Fang, P., Pastor-Soler, N., Brown, D., & Van Hoek, A. N. (2004). Membrane organization and function of M1 and M23 isoforms of aquaporin-4 in epithelial cells. *American Journal of Physiology. Renal Physiology*, *287*, F501–F511.

Simone, L., Pisani, F., Mola, M. G., De Bellis, M., Merla, G., Micale, L., Frigeri, A., Vescovi, A. L., Svelto, M., & Nicchia, G. P. (2019). AQP4 aggregation state is a determinant for glioma cell fate. *Cancer Research*, *79*, 2182–2194.

Skucas, V. A., Mathews, I. B., Yang, J., Cheng, Q., Treister, A., Duffy, A. M., Verkman, A. S., Hempstead, B. L., Wood, M. A., Binder, D. K., & Scharfman, H. E. (2011). Impairment of select forms of spatial memory and neurotrophin-dependent synaptic plasticity by deletion of glial aquaporin-4. *The Journal of Neuroscience*, *31*, 6392–6397.

Sloan, S. A., & Barres, B. A. (2014). Mechanisms of astrocyte development and their contributions to neurodevelopmental disorders. *Current Opinion in Neurobiology*, *27*, 75–81.

Smith, A. J., Jin, B.-J., Ratelade, J., & Verkman, A. S. (2014). Aggregation state determines the localization and function of M1- and M23-aquaporin-4 in astrocytes. *The Journal of Cell Biology*, *204*, 559–573.

Sofroniew, M. V., & Vinters, H. V. (2010). Astrocytes: Biology and pathology. *Acta Neuropathologica*, *119*, 7–35.

Solenov, E., Watanabe, H., Manley, G. T., & Verkman, A. S. (2004). Sevenfold-reduced osmotic water permeability in primary astrocyte cultures from AQP-4-deficient mice, measured by a fluorescence quenching method. *American Journal of Physiology. Cell Physiology*, *286*, C426–C432.

Sorbo, J. G., Moe, S. E., Ottersen, O. P., & Holen, T. (2008). The molecular composition of square arrays. *Biochemistry*, *47*, 2631–2637.

Striedinger, K., Meda, P., & Scemes, E. (2007). Exocytosis of ATP from astrocyte progenitors modulates spontaneous Ca2+ oscillations and cell migration. *Glia*, *55*, 652.

Striedinger, K., & Scemes, E. (2008). Interleukin-1beta affects calcium signaling and in vitro cell migration of astrocyte progenitors. *Journal of Neuroimmunology*, *196*, 116–123.

Strohschein, S., Hüttmann, K., Gabriel, S., Binder, D. K., Heinemann, U., & Steinhäuser, C. (2011). Impact of aquaporin-4 channels on K+ buffering and gap junction coupling in the hippocampus. *Glia*, *59*, 973–980.

Stubbs, D., Deproto, J., Nie, K., Englund, C., Mahmud, I., Hevner, R., & Molnár, Z. (2009). Neurovascular congruence during cerebral cortical development. *Cerebral Cortex*, *19*, i32–i41.

Syková, E., Mazel, T., & Šimonová, Z. (1998). Diffusion constraints and neuron-glia interaction during aging. *Experimental Gerontology*, *33*, 837–851.

Toft-Bertelsen, T. L., Križaj, D., & MacAulay, N. (2017). When size matters: Transient receptor potential vanilloid 4 channel as a volume-sensor rather than an osmo-sensor. *The Journal of Physiology*, *595*, 3287–3302.

Toft-Bertelsen, T. L., Larsen, B. R., & MacAulay, N. (2018). Sensing and regulation of cell volume – We know so much and yet understand so little: TRPV4 as a sensor of volume changes but possibly without a volume-regulatory role? *Channels*, *12*, 100.

Verkman, A. S., Anderson, M. O., & Papadopoulos, M. C. (2014). Aquaporins: important but elusive drug targets. *Nature Reviews. Drug Discovery*, *13*, 259–277.

Verkman, A. S., Rossi, A., & Crane, J. M. (2012). Live-cell imaging of aquaporin-4 supramolecular assembly and diffusion. *Methods in Enzymology*, *504*, 341–354.

Von Visger, J. R., Yeon, D. S., Oh, T. H., & Markelonis, G. J. (1994). Differentiation and maturation of astrocytes derived from neuroepithelial progenitor cells in culture. *Experimental Neurology*, *128*, 34–40.

Weidman, T. A., & Kuwabara, T. (1968). Postnatal development of the rat retina. An electron microscopic study. *Archives of Ophthalmology*, *79*, 470–484.

Wen, H., Nagelhus, E. A., Amiry-Moghaddam, M., Agre, P., Ottersen, O. P., & Nielsen, S. (1999). Ontogeny of water transport in rat brain: Postnatal expression of the aquaporin-4 water channel. *The European Journal of Neuroscience*, *11*, 935–945.

Wise, S. P., & Jones, E. G. (1976). The organization and postnatal development of the commissural projection of the rat somatic sensory cortex. *The Journal of Comparative Neurology*, *168*, 313–343.

Yao, X., Hrabětová, S., Nicholson, C., & Manley, G. T. (2008). Aquaporin-4-deficient mice have increased extracellular space without tortuosity change. *The Journal of Neuroscience*, *28*, 5460–5464.

Yoneda, M., Nishizaki, T., Tasaka, K., Kurachi, H., Miyake, A., & Murata, Y. (2000). Changes in Actin network during calcium-induced exocytosis

in permeabilized GH3 cells: Calcium directly regulates F-Actin disassembly. *The Journal of Endocrinology*, *166*, 677–687.

Zecevic, N. (2004). Specific characteristic of radial glia in the human fetal telencephalon. *Glia*, *48*, 27–35.

Zeng, X. N., Sun, X. L., Gao, L., Fan, Y., Ding, J. H., & Hu, G. (2007). Aquaporin-4 deficiency down-regulates glutamate uptake and GLT-1 expression in astrocytes. *Molecular and Cellular Neurosciences*, *34*, 34–39.

Zhang, J., Li, Y., Chen, Z. G., Dang, H., Ding, J. H., Fan, Y., & Hu, G. (2013). Glia protein aquaporin-4 regulates aversive motivation of spatial memory in Morris water maze. *CNS Neuroscience & Therapeutics*, *19*, 937–944.

Zheng, G. q., Li, Y., Gu, Y., Chen, X. m., Zhou, Y., Zhao, S. z., & Shen, J. (2010). Beyond water channel: Aquaporin-4 in adult neurogenesis. *Neurochemistry International*, *56*, 651–654.

SUPPORTING INFORMATION

Additional supporting information can be found online in the Supporting Information section at the end of this article.

How to cite this article: Cibelli, A., Mola, M. G., Saracino, E., Barile, B., Abbrescia, P., Mogni, G., Spray, D. C., Scemes, E., Rossi, A., Spennato, D., Svelto, M., Frigeri, A., Benfenati, V., & Nicchia, G. P. (2024). Aquaporin-4 and transient receptor potential vanilloid 4 balance in early postnatal neurodevelopment. *Glia*, *72*(5), 938–959. https://doi.org/10.1002/glia.24512